Stuck Pipe Early Warning System Utilizing Moving Window Machine Learning Approach

Omogbolahan S. Ahmed, Beshir M. Aman, Majed A. Zahrani, and Folorunsho I. Ajikobi

Abstract /

As stuck pipes continue to be a major contributor to nonproductive time (NPT) in drilling operations for oil and gas, efforts to mitigate this incident cannot be over emphasized. A machine learning approach is presented in this article to identify warning signals and provide early indications for an impending stuck pipe possibility during drilling activities, so as to take proactive measures to mitigate its occurrence.

The model uses a moving window-based approach to capture key drilling parameter trends and apply an unsupervised machine learning algorithm to predict abnormalities in the parameters' rate of change. It utilizes most commonly available drilling real-time data, and is therefore deployable in all types of wells. No pre-drill model is essentially required as the system utilizes a self-learning and self-adjusting model.

The methodology involves the use of change point detection in identifying rig activity and the associated drilling parameters to capture relevant parametric trends for analysis. Inherent in the parameter trend are the different factors that affects their readings; such as wellbore geometry, bottom-hole assembly (BHA), dogleg severity (DLS), formation characteristics, pump flow rate, and pipe rotations.

The algorithm has been tested on data from historical wells in which stuck pipe incidents, near-miss stuck pipes, and incident-free wells occurred to prove the concept. The results of the model performance is hereby presented along with an accuracy measure.

Introduction

Stuck pipe prediction and mitigation strategies has and will continue to receive attention in the drilling for oil and gas as more complex wells are being drilled across depleted zones to reach deeper reservoir targets. Early detection of a stuck pipe and mitigating the incident in real time not only helps to prevent its occurrence, but also helps in making informed decisions as to the appropriate freeing mechanism to adopt if it occurs.

Oftentimes, when a stuck pipe incident occurs, costly corrective actions may include fishing operations, sidetracking the hole, or completely having to drill a new well[1]. Therefore, various industry estimates claiming that stuck pipe costs may exceed several hundred million dollars per year is not far-fetched. Stuck pipe incidents account for a substantial part of nonproductive time (NPT), with estimates ranging from 25% to 35%[2].

Understanding stuck pipe mechanisms and their classic signatures helps in the early detection of the trends, and helps in proactively deploying mitigating strategies against an impending incident. Due to short human memory, crew changes during drilling operations and trivial parameter trends, among other factors, stuck pipe warning signs are often undetected early enough for the deployment of effective mitigation strategies.

In this study — a machine learning approach — a moving window-based regression model is used to develop a system for detecting early warning signs of common stuck pipe mechanisms during drilling operations. The unsupervised machine learning algorithm is programmed to automatically detect abnormalities in real-time drilling parameter trends and predict potential stuck pipes, communicate observations in the form of alerts to engineers in advance to allow for proactive corrective actions. This invariably increases the chance of avoiding severe sticking in the first place and success in timely freeing the pipe if at all it happened. Since stuck pipe incidents account for a substantial part of NPT, time is crucial in such cases as an improper reaction to a stuck pipe incident can easily make it worse.

Major causes of stuck pipes in drilling for oil and gas operations includes key seating, improper mud control, excessive overbalance, cuttings accumulation, cuttings or sand avalanche, shale cavings, and balling up. Early identification of the stuck mechanism leads to deploying the relevant preventative measures such as recommendations, which deals with drilling practices — and are abundant in literature. For example, maintaining wellbore stability, avoiding wellbore tortuosity, running a reamer in the bottom-hole assembly (BHA), avoiding improper mud control by ensuring proper cuttings suspension, providing low filtration rates into the formation, and avoiding excessively thick filter cakes[3].

As a well is being drilled, it is always in communication with the driller using telltale signs from drilling parameters. The telltale means of communicating its condition as it relates to impending stuck pipe while drilling

is in the understanding of the behavior of three principal surface parameters; they are hook load (HKLD), rotary torque (TRQ), and standpipe pressure (SPP). The understanding of the expected trend of these easily accessible parameters goes a long way in early detection, and therefore, mitigation of stuck pipe. We listen to the well by monitoring the trends of these parameters during drilling and tripping operations.

The system and methodology hereby presented, strives to contribute to the foundation's building block of drilling automation by automating the trend analysis and monitoring of HKLD, TRQ, and SPP while drilling, tripping or back reaming in any type of well to identify key signatures of impending stuck pipe. The system keeps a log of all stuck pipe signals as so-called observations during different drilling activities and the corresponding depths which could be used to gauge the hole condition with time. As drilling progresses with cumulative observations, the stuck pipe severity indices increase, leading to the generation of alerts, which will prompt the driller or engineer to activate mitigating strategy to avert a stuck pipe incident.

Drilling Parameters Trend Analysis

A major factor in successfully drilling a well, free of a stuck pipe incident, is the ability to critically and continuously monitor multiple drilling and tripping parameter trends for early detection of abnormalities. A trend is defined as the direction of change of one parameter with respect to another in relation to a reference point.

Deploying machine learning in drilling parameter trend analysis has become increasingly popular due to its obvious advantages over human limitations in simultaneous multiple parameters trend analysis, which occurs as a results of short memory span, short attention and concentration span, crew and shift changes, deducing subtle but critical changes in parameters and their relationships, which are often not linear, etc. Machine learning approaches also offers automated solutions to these limitations, and with artificial intelligence, can adapt human knowledge to mitigate stuck pipe occurrences.

In trend analysis, it is not so much the value of any of the parameters that matters. It is the direction of change in one of these parameters with respect to others. Trend analysis is relational; therefore, it must involve at least two parameters.

Analysis of Surface Drilling Parameters

Understanding the relationship and expected behavior of some key surface drilling mechanics parameters is a necessity in analyzing wellbore condition in real-time. The general practice is for an optimization engineer to develop a torque and drag simulation model simulating the HKLD and TRQ over measured depth, based on a specific BHA, mud rheology, and wellbore trajectories. The methodology being proposed in this work, however, does not negate the importance of simulation models, but rather would complement it in proactively identifying an anomaly in wellbore condition and mitigate a stuck pipe incident before it occurs.

An increase or decrease in friction of the drillstring lowered into the wellbore can be identified through the real-time trend of the measured HKLD, as it is much more important to monitor the trend of the HKLD development than to compare it to one specific calculated ideal value[4]. This is because it is more difficult to define what an expected "normal" HKLD is due to various interacting dynamic forces acting on the drillstring. The simulation calculated the maximum and minimum HKLD while pulling out of the hole (POOH) and running in the hole (RIH), respectively. Differential sticking can easily be detected when the out-of-slips HKLD trend is tracked for both POOH and RIH. Among other signals, a classic warning sign of impending differential stuck pipe is that the out-of-slips HKLD peak will show a continuously increasing trend from one connection to the next during the drilling operation.

The surface TRQ also responds to a worsening hole condition in a similar fashion. The same procedures and principle are applicable for the surface TRQ. Another classical signature of potential differential sticking is a spike in TRQ after a period of non-pipe movement. Additionally, the increasing off bottom rotary TRQ could also be an indication of increasing friction in the hole due to poor hole cleaning or tight hole conditions. Being able to track these automatically gives the driller or engineer an advantage of proactive remedial action to prevent a stuck pipe.

Detecting a Developing Stuck Pipe during Drilling

For proper trend analysis while the drilling operation is ongoing, it is important to monitor the pickup and slack off weights without rotation. These values can normally be measured before breaking the stand for a new connection. To judge the downhole situation, it is much better to use HKLDs from string movements without rotation, because this is when the full friction is acting against the axial movement and its influence on the HKLD is at its maximum.

Mechanical Sticking Mechanism

A major problem in deviated, extended reach drilling and horizontal sections is the buildup of a cuttings bed in the annulus. A persistent increase in friction — until the string is stuck and the hole is lost — is the resultant effect of the cuttings bed build up, due to poor hole cleaning.

This unwanted situation can be detected early by constant, automated, real-time monitoring and analysis of the trend of the measured HKLD, TRQ, and SPP for successive stands drilled. This will enable the drilling team to activate mitigating countermeasures early to avoid the potential costly lost time due to a preventable stuck pipe.

Differential Sticking Mechanism

Differential pipe sticking tendency is the increase of the friction between the drillstring and the wellbore wall due to high overbalance pressure between the hydrostatic and formation pressure. This results in increased forces acting on the drillstring against the wellbore. As previously described, the sticking tendency increases over time, and therefore, a differential stuck pipe situation may emerge

over hours. It can be detected early by monitoring the out of slip pickup weights during connections in real time. This monitors the increasing trend of the inertial of the drillpipe after a period of non-movement.

Automating this process will help the drillers and engineers to identify early the trend of increasing out of slips weights, and therefore, proactively mitigate the impending stuck pipe. A classic signature of increasing inertial to movement, is the spike in TRQ when rotation is established after a period of non-movement of the drilling strings.

Detecting a Developing Stuck Pipe during Tripping

A tripping operation can be defined as the operations involved in moving the BHA in or out of a hole that has been drilled. This could either be RIH to resume drilling and condition the hole; or POOH to change the BHA and wipe the hole after drilling. Monitoring the evolution of friction by using the torque and HKLD trend while tripping will provide insights into the wellbore condition in terms of aging, and the worsening of trouble zones. Some of the major stuck pipe causative agents that can be identified during tripping operations includes, but is not limited to the following: development of ledges, key seats, and tight holes.

Ledges occurred while drilling through alternating hard and soft formations, and naturally fractured formations. Stabilizers in the BHA and tool joint easily wear through soft formations and naturally fractured formations while the hard formations remain engaged. Classic identification of ledges during a tripping operation is the cyclic erratic overpull observed when tripping in or out of the hole and during connections, sudden set down (decrease in HKLD) as the drillstring or casing runs into a ledge while RIH. The trend of these HKLD readings over several trips is of great interest as it provides a visual impression of the evolution of the ledges over time. This gives the driller an advance warning to activate a mitigation strategy.

Keyseats occur as drillstrings cut into the formation due to an increase in side forces at areas of high doglegs or ledges. During tripping operations, the development of key seats can be monitored, especially at intervals of potential formation of key seats. Classic signatures of a key seat include an increase in TRQ and drag while drilling or tripping. Cyclic drag can happen while tripping as there may be overpull spikes when tool joints are pulled through keyseats. A progressive increase in overpull on subsequent trips through the same interval of the hole is a confirmation of a developed keyseat[5].

Tight hole problems related to the formation as a result of wellbore instabilities closes the annulus around the drillstring; this is quite similar to forming a keyseat. When tripping through the same formation, the HKLD behavior is such that it is lower than normal when RIH, and if overpull is encountered while POOH, then the formation should be closely monitored. Aging of the wellbore, if no remedial action is taken, worsens the situation. The solution may be to ream this formation until the HKLD is back to normal when tripping through the formation or revise the mud weight for wellbore stability.

An intelligent system can automatically track and analyze parameter trends, alert the driller or drilling engineer early so that countermeasures can be taken before the string gets stuck.

Data Description and Selection

Utilization of sensor technology in the drilling industry has enabled the collection of real-time drilling parameter data and has made so many analyses possible, be it during execution or post well analysis. For instance, the state of the drilling operation could be autonomously communicated remotely to concerned parties on a per second basis; it is also a foundation for autonomous drilling. Saudi Aramco has been an industry leader in the use of real-time drilling data for optimal well placement, improving drilling efficiency, reducing operational risk and optimizing drilling processes. The drilling real-time data hub is the WITSML Oracle database, which has been populated with data from thousands of wells since 2008[6].

Historical real-time drilling parameter data from 10 wells, where five of them had a stuck pipe incident of different mechanisms, were collected from the drilling real-time data hub. The data quality of the wells were categorized as good to excellent based on the following criteria: "completeness (the degree to which each sensor data point contains the expected readings), sensibility (the degree to which the sensor reading values conform to certain quality thresholds), uniformity (the degree to which the streamed volume of sensor data points is consistent over time), and structure (the degree to which streamed data points conform to an agreed upon structure)"[6].

For versatility, the alerting system is being designed to cater for different well and rig types provided, even if only "critical" drilling parameter streams are available. There are many parameters to consider in drilling, but the most important parameters with respect to our study are: HKLD, hook block height (HKHT), rotary speed per minute (RPM), TRQ, SPP, flow rate, rate of penetration, weight on bit, hole depth, bit depth, hole inclination, and dogleg severity (DLS).

Methodology

In this section, the overall methodology of the developed model will be highlighted and the underlying components will be further explained in subsequent sections.

Model Flowchart

Figure 1 illustrates the stuck pipe model's flowchart. Once real-time data is generated, it will be processed by the rig state identification method and produce appropriate codes for the current state. In addition, records with nonphysical parameters or out of range values will be marked as invalid parameters and are excluded from any further calculations. Afterwards, an algorithm to find the next pickup point after a connection state will be applied. Next, a number of algorithms will be executed to look for different symptoms related to stuck pipe events.

If any defined symptoms are found, the model will produce an observation with a log summarizing underlying

Fig. 1 *Stuck pipe model flowchart.*

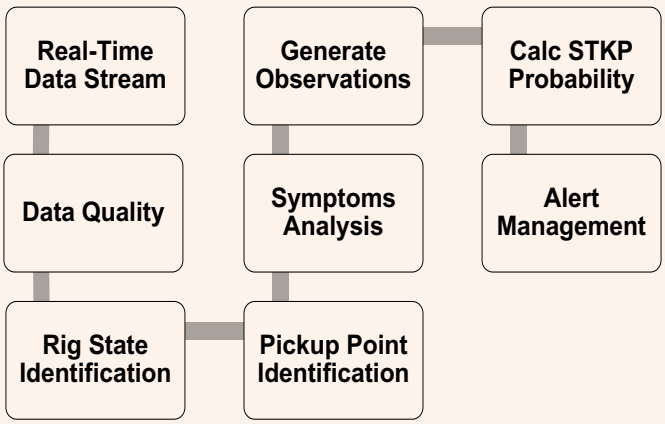

symptoms, which is visible to drilling engineers. The model will calculate the stuck pipe probability based on the presence of one or more observations. Eventually, an alert will be generated if the stuck pipe probability exceeds certain thresholds, taking into consideration the frequency of such symptoms in a given time frame and the type of current rig state.

Rig State Identification

In this work, the presented method evaluates the pickup weight right after each drillpipe connection as an indicator of some types of potential hole troubles. This task requires a precise identification for the end of the connection operation. For this, a rig state identification method is used[7,8]. Since most rig state identification methods decode the operation at a microscale level, i.e., each transmitted WITSML record is evaluated independently from existing records.

Due to this low level of classification, these methods can have a high level of noise in which some non-connection operations are classified as a connection, and a true connection operation might contain non-connection operation records in between. To overcome this problem, we enhance the accuracy of the rig state identification method by applying a change point detection algorithm[9] to the identified rig states.

The change point detection algorithm uses two sliding windows of equal length, then, using a distribution divergence distance measure we evaluate the distance between the data within these sliding windows using Eqn. 1:

$$d_t = \sum |c_{1i} - c_{2i}| \quad (1)$$

where c_1 and c_2 are the frequency of classification code (i) in left and right sliding windows, respectively. The change point detection algorithm will try to find the time point (t) that maximizes this value, Fig. 2.

Pickup Point Identification

The rig state provides operation code in real-time, including connection time. The model will capture HKLD readings at the pickup points, i.e., points right after the "connection" code. Assuming that the BHA is fixed, the pump flow rate is fixed at a certain level, the pipe is rotating at a certain level (RPM is fixed), and we are tripping on a vertical well.

The HKLD readings at subsequent pickup points will increase at a certain rate due to adding one stand at a time, and vice versa while tripping out. What is more, HKLD readings for a horizontal well will be less compared to a vertical one due to gravity forces. Figure 3 is an example of identified pickup points for the given HKLD points.

HKLD at Pickup Points Symptoms

The behavior of the HKLD at pickup points usually follows Eqn. 2:

$$HKLDt_n = HKLDt_{n-1} \pm x \quad (2)$$

where

$HKLDt_n$: The HKLD reading at current pickup point at time, t_n

$HKLDt_{n-1}$: The HKLD reading at a previous pickup point at time, t_{n-1}

x: The change rate, positive and negative rates refer to tripping in and out, respectively.

The model will take some time initially to learn the block weight position at the connection times and identify the first 10 pickup points. Then, it will implement a moving window regression algorithm on the last 10 HKLD readings to learn a new pattern as:

$$HKLDt_{n-10:}t_n \sim RIGTIMEt_{n-10:}t_n \quad (3)$$

where

$HKLDt_{n-10:}t_n$: The HKLD readings for the last 10 pickup points at rig time, i.e., t_{n-10}, t_{n-9}, …, t_n

$RIGTIMEt_{n-10:}t_n$: The rig time for the last 10 pickup points, i.e., t_{n-10}, t_{n-9}, …, t_n

The idea here is to compute the HKLD change rate, x, in real-time for the last 10 pickup points. Then, predict the subsequent HKLD value ($\widehat{HKLDt}_{n+1}$) and compare it

with the upcoming pickup point, $HKLDt_{n+1}$. Afterwards, the model will identify if the actual reading exceded a certain threshold, e.g., 10% of the estimated one.

By doing so, this will handle the trajectory factor since recent points will have a similar angle. In addition, the time series is re-initialized automatically whenever there is a change in the RPM, and the flow in rate.

Another symptom, i.e., the HKLD inverse direction,

Fig. 2 *Change point detection algorithm. The black line is the input data stream, the green and blue boxes are the right and left sliding window, respectively, and the red line is the calculated distribution divergence distance for data from both sliding windows evaluated at their adjacent point.*

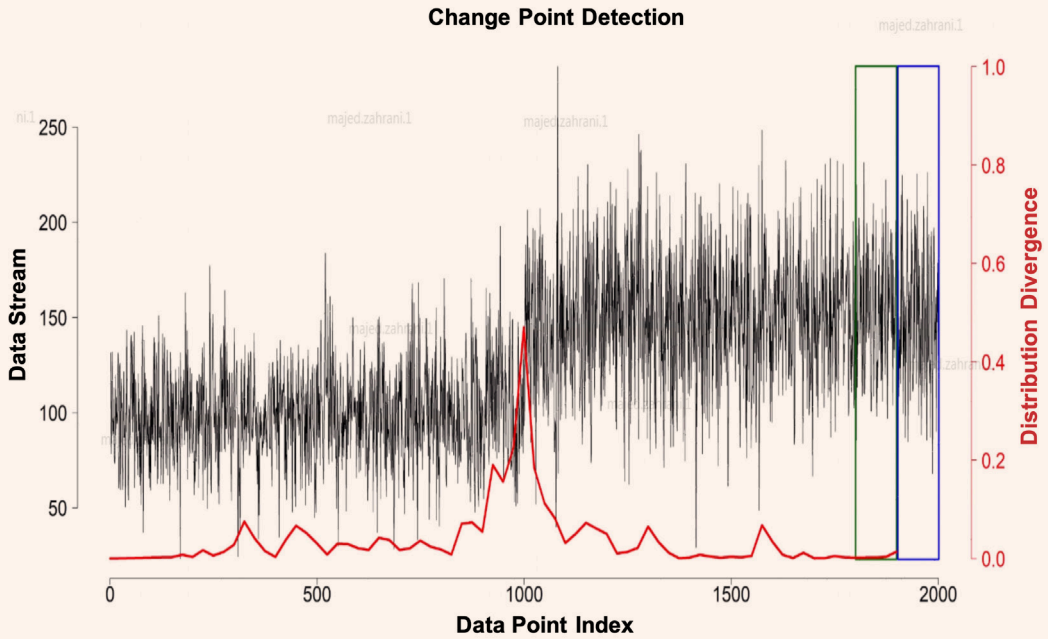

Fig. 3 *The identification of the pickup points and the corresponding HKLD readings.*

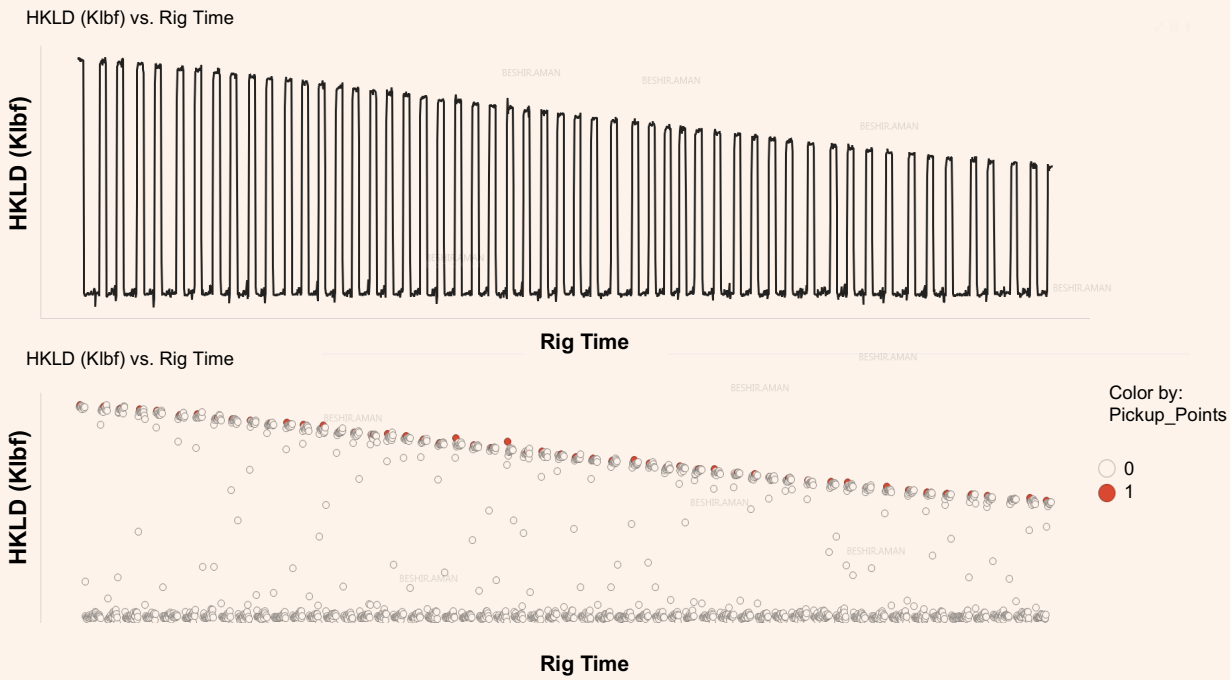

can be identified by utilizing the slope of the moving window regression. For example, the HKLD value usually decreases during the tripping out activity. Subsequently, if it started to be flat or even increase, this might indicate an over pull. In this case, the model will indicate this abnormality when the slope is different than expected, i.e., in this case, a non-negative slope value.

HKLD Spikes between Connections Symptom

The HKLD usually settles to a certain level between two connections. The model will look for spikes where it will exceed a certain threshold percentage in either direction. Each point in the current interval will be compared to the HKLD level at the previous interval by computing a median statistic. The median value has an advantage over the simple average since it will not be affected by outliers.

Figure 4 is an example of the HKLD jumps. Once the HKLD spike is detected, a summary of this symptom will be recorded for further analysis.

Non-Smooth HKHT Symptom

The HKHT movement should be smooth while tripping in general. There are many reasons why the HKHT is not smooth, some of which may or may not contribute to stuck pipe. Examples include: going back and forth while RIH or POOH, performing hole cleaning activities, or even staying stationary. Therefore, a symptom is considered to identify such cases where it will be significant only if it occurs simultaneously with other symptoms. Two regression models were utilized to analyze the smoothness of the HKHT between two connections at a time: one considers the major activity only, e.g., tripping in, and the other considers all activities, including the major one. In case there are no minor activities, both models will have a similar slope. In case there are other activities along with the major one, the two slopes will significantly differ, thereby indicating non-smoothness in the HKHT. Figure 5 shows an example of the non-smooth HKHT movement detected by the model.

SPP Increase Symptom

Part of the model objective is to capture sudden changes in the trend of the SPP. This is achievable by monitoring the change in the trend of the SPP along with the corresponding flow rate parameters over time. The model will track a moving window of recent SPP values and predict the next SPP value using linear regression with a defined envelope. If the new actual value exceeds the envelope, then the model will check for the flow rate behavior. If it also had sudden changes, it will capture it as normal, otherwise, it will be recorded as an observation. With this observation, potential park-off tendency in a well can be detected early.

TRQ Spikes Symptom

In this symptom, we monitor a moving window of recent TRQ changes right after connection and when the RPM is on. By doing so, this will help track the trend of string movement inertia. Afterwards, the next TRQ value is predicted with a defined envelope using linear regression, and is compared with upcoming actual value.

This inertia provides an indication of increasing friction in the well and drilling string resistance to move after a period of non-movement. If the new value exceeds the envelope, it will be marked as an observation. Evolving differential sticking tendency and poor hole cleaning can be detected and addressed early with this symptom.

DLS Indicator

Usually, a survey is taken at every one stand to measure

Fig. 4 *An identified system alert for increasing the overpull after connections and HKLD jumps between the connections.*

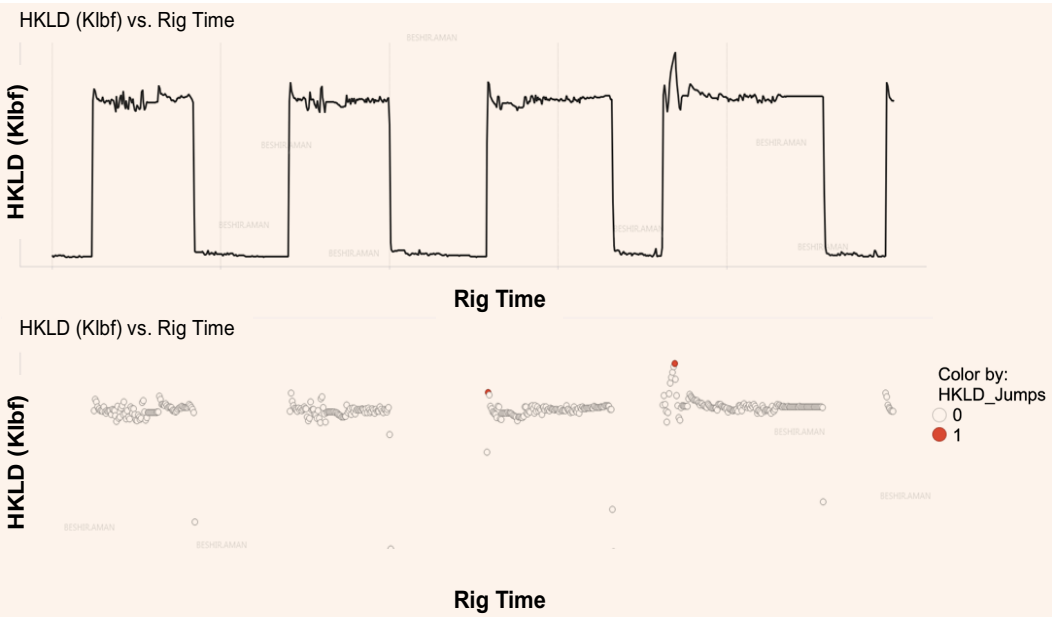

Fig. 5 *Typical HKHT, HKLD, and HKHT non-smooth behavior symptoms of a hole condition during tripping or drilling operations, detected by the model.*

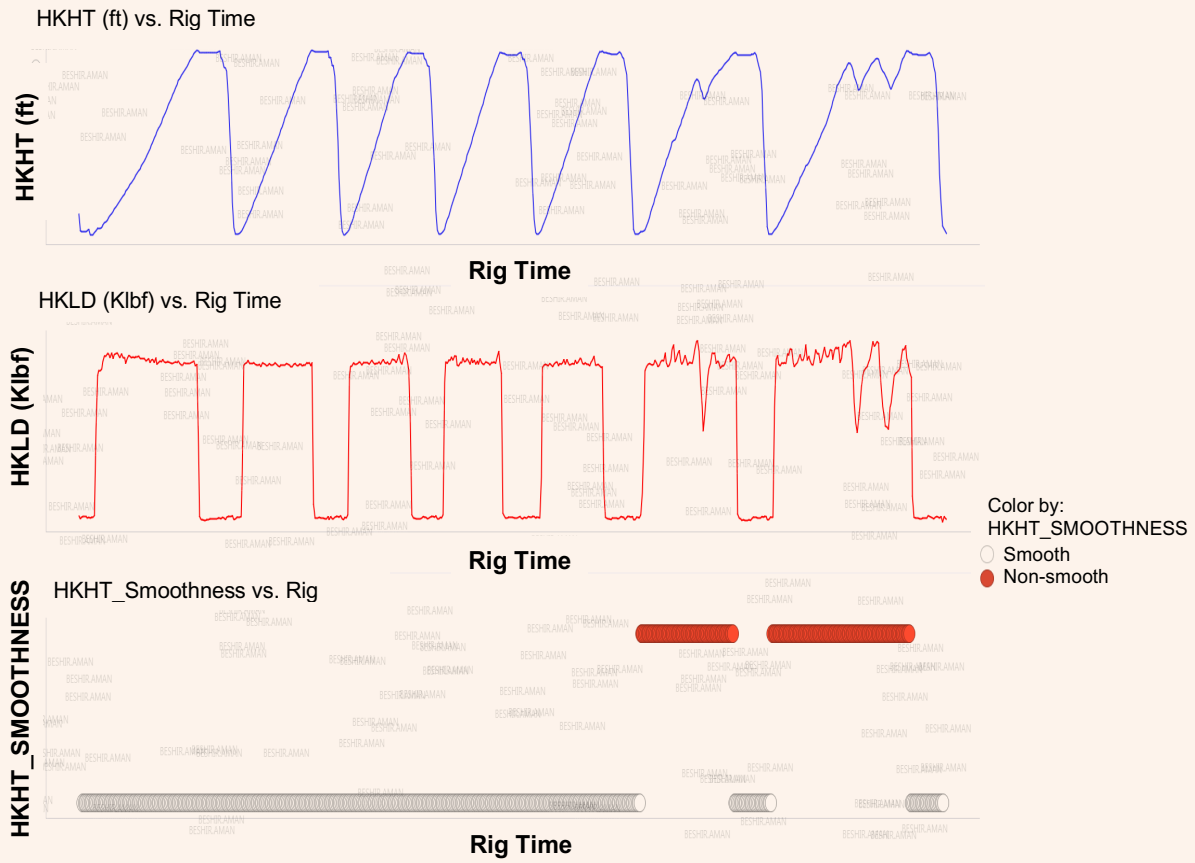

different parameters, including DLS, azimuth, and inclination at a given measured depth. A high DLS, above about 3° value, can be problematic, and especially while conducting tripping activities if it is not consistent with planned DLS. The model will generate an observation whenever drillpipe bit depth is within one stand and a half in either direction of any identified high DLS point. This will take into account the BHA component's size and length, in addition to any uncertainty in the DLS value in between the survey points.

Stuck Pipe Probability

After analyzing the observed symptoms along with their descriptive summary, the stuck pipe probability is calculated based on the current operation, and the sum of the assigned weights to the observed symptoms.

To come up with the stuck pipe probability, the different symptoms previously described are assigned weights based on the prevalent rig activity at the time the observations were logged. These weightings can be obtained statistically based on the frequency of the appearance of each symptom. In this study, we have assigned weightings to each symptom based on their importance to identifying potential stuck pipe within the prevailing rig activity, Table 1. For example, while tripping in activity, the relevant combination of stuck pipe symptoms are: non-increasing HKLD (increasing set down weight), HKLD spikes, non-smooth HKHT, and TRQ spikes right after positive RPM and high DLS. Then, symptoms with higher importance are given larger weights.

Stuck Pipe Alert

Now, the stuck pipe probability is estimated based on the aggregation of the weighted sum of simultaneously observed symptoms. An alert is therefore raised or generated if the aggregate exceeds a certain threshold. In this study, an aggregate of 0.60 was used to raise an alert.

Cases and Discussions

Four case studies are hereby presented to demonstrate the ability of the model/system to differentiate early warning symptoms of impending stuck pipe. It further demonstrates the fact that most stuck pipes are preventable if detected early enough and if a mitigation strategy is deployed on time.

Case 1

In this case, archived real-time data from Well-A was ran through the model in a playback mode. Well-A was known to have a mechanical stuck pipe. As can be seen in Fig. 6, the model generated several observations set to be detectable by the model while RIH with a new BHA. The severity and probability of the stuck pipe shows an

Table 1 *Weights that can be used to calculate the probability of a stuck pipe.*

Symptom/Activity	Tripping Out	Tripping In	Drilling
HKLD increase at pickup points	0.20	—	—
HKLD inverse direction	—	0.20	—
HKLD spikes between connections	0.20	0.30	0.25
HKHT is non-smooth	0.10	0.10	—
SPP increase while flow rate is steady	0.20	—	0.25
TRQ spikes as RPM is switched on	0.20	0.30	0.25
DLS	0.10	0.10	0.25
Total	1.00	1.00	1.00

Fig. 6 *Two stuck pipe alerts with high probability prior to an incident in Well-A. Highlighted abnormalities included a high DLS value, and an overpull of more than 25 Klbf than the previous HKLD level while RIH.*

increasing trend as we approach the stuck point.

Two alerts were generated by the system prior to the stuck pipe incident. Although these alerts were in retrospect, they were generated in playback mode of the real-time data, meaning that if this model was deployed during the execution of the well, it would have spotted the anomalous trend and alerted the concerned parties to take mitigating actions to avert the stuck pipe incident, thereby saving the operator costly NPT.

Case 2

In the second example, archived real-time surface drilling data from Well-B was ran through the model, also in a playback mode. Just as in the first case presented, several observations were made with varying degrees of severity based on the aggregate weights of the observations. The major activity in this well was also RIH after a bit change.

Figure 7 shows an alert was generated prior to the stuck pipe incident, which further demonstrated that this incident was preventable if detected early and mitigating strategy was timely deployed.

Case 3

In this example, the archived real-time data from Well-C was also ran through the model. In this particular case, after drilling to the casing point and circulating the hole clean, the POOH was slick and the system did not generate any false alerts. As can be seen in Fig. 8, some valid observations of DLS and non-smoothness of

Fig. 7 *A stuck pipe alert with high probability prior to the incident in Well-B. The highlighted abnormalities included high DLS value, and a non-increasing HKLD value compared to previous levels while RIH.*

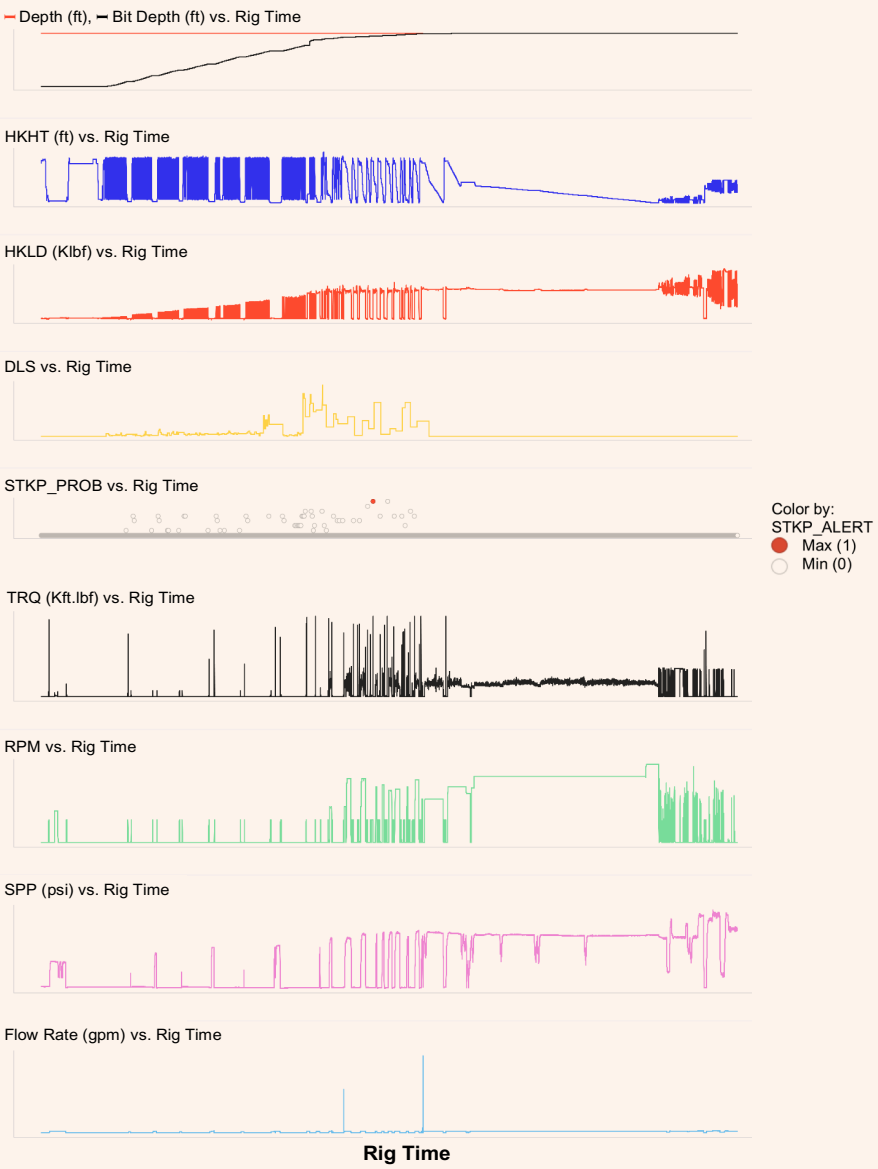

Fig. 8 *Well-C is used as an example for a control case.*

HKHT were made, but no abnormal trend in HKLD or TRQ were seen simultaneously. Therefore, based on the weightings of the symptoms, the aggregate sum was not enough to generate an alert.

We have used this case along with others as a control and measure of reliability for the alerting system so as to reduce the generation of false alerts as much as possible.

Case 4

The fourth case presented was Well-D, which had a differential stuck pipe after spending excess time in slips during connection. The archived real-time data of the well was run in playback mode through the model to see if classic warning signs of differential stuck pipe were present before the incident occurred. The system generated three alerts and several observations, which included spikes in TRQ, associated with the initial rotation after connections of more than three stands prior to the stuck incident, Fig. 9.

There were also simultaneous overpull corresponding to these observations. The aggregate sum of these simultaneous observations may not reach the threshold to send alerts, therefore it is important to know the prevailing stuck pipe risk and adjust the weighting accordingly. For instance, if we know we are drilling with high overbalance across permeable zones, we are prone to differential sticking and can therefore increase the weightings of the corresponding symptoms so as not to miss early alerts.

Conclusions and Recommendations

We have presented a methodology using the moving

Fig. 9 *Three stuck pipe alerts with high probability generated prior to the incident in Well-D. Classic signatures of differential stuck pipe tendency were captured prior to the stuck pipe incident while drilling.*

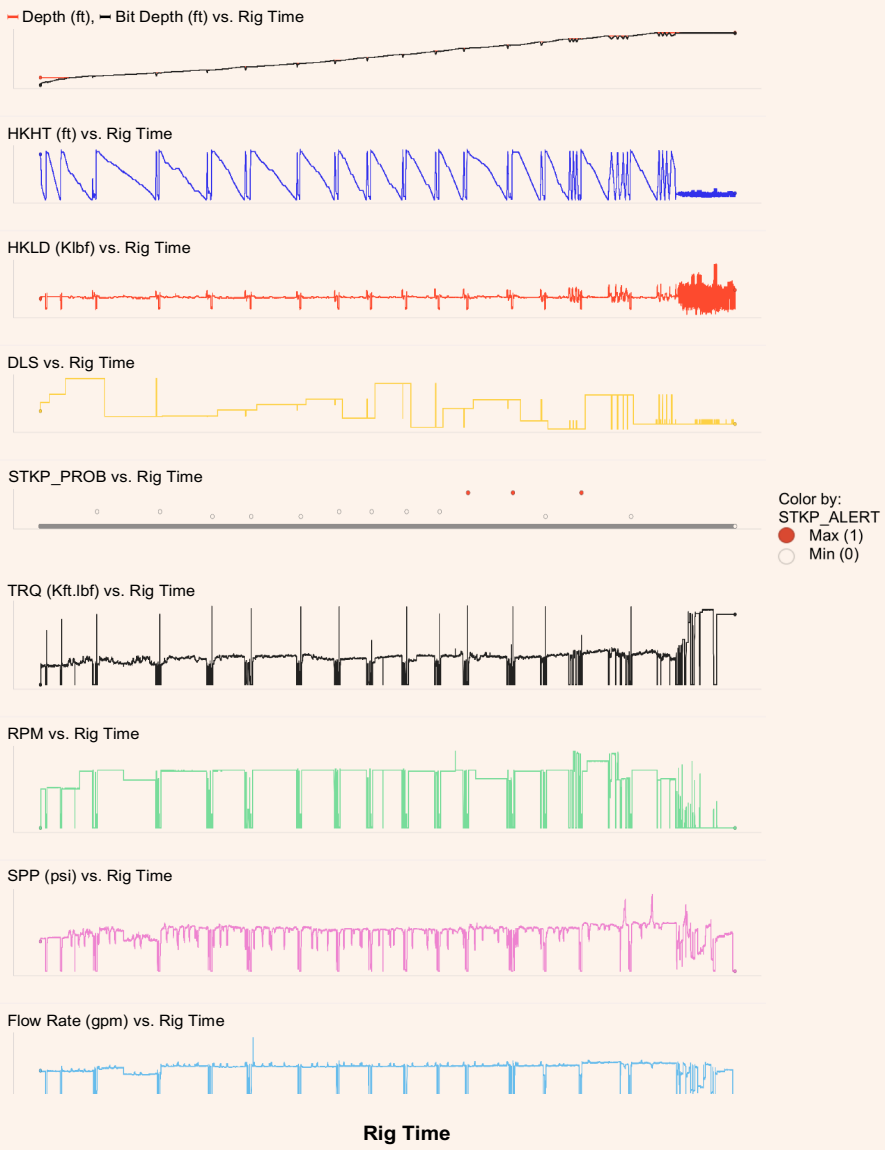

window linear regression approach to capture and monitor the trend of drilling parameters directed at capturing classic warning signatures of stuck pipe. As a well is being drilled, it is believed to be communicating its condition to the driller. The model presented in this study has demonstrated that listening to the well can be automated and early warning signs of stuck pipe can be deciphered from the drilling parameters.

In the case studies presented, several warning signatures were picked and alerts raised before the stuck pipes occurred. Consequently, as historical data were used in playback mode for this study, the same approach is applicable for real-time well monitoring. For operational reasons, one or two of the alerts captured in this study were false; nonetheless, the model shows an overall promising result with a precision of 0.67, and a sensitivity of 0.8 for the 10 wells used to prove this concept.

As every well is unique in design and complexity, so also will their stuck pipe mechanism risk factors differ. When drilling through depleted zones, differential stuck pipe risk factors are high, therefore, the weighting for the symptoms that aids in the early detection of differential stuck pipe should be higher. In extended reach drilling, symptoms that detects poor hole cleaning may have higher weightings. Therefore, knowledge of the uniqueness of the well is important in deploying and adapting the methodology hereby presented.

In our future work, this approach will be further enhanced by refining existing symptoms, including more symptoms and scenarios, and optimizing the model performance for real-time deployment, which will eventually help reduce the uncertainty of stuck pipe probability.

Acknowledgments

This article was prepared for presentation at the Abu Dhabi International Petroleum Exhibition and Conference, Abu Dhabi, UAE, November 9-12, 2020.

References

1. Abd Elsalam, H., ElNady, Y., Elfakharany, T. and Dahab, A.S.: "Systemic Approach to Minimize Stuck Pipe Incidents in Oil Wells," *Journal of Al Azhar University Engineering Sector*, Vol. 11, Issue 38, Winter 2016, pp. 255-264.

2. Muqeem, M.A., Weekse, A.E. and Al-Hajji, A.A.: "Stuck Pipe Best Practices — A Challenging Approach to Reducing Stuck Pipe Costs," SPE paper 160845, presented at the SPE Saudi Arabia Section Technical Symposium and Exhibition, al-Khobar, Saudi Arabia, April 8-11, 2012.

3. Salminen, K., Cheatham, C., Smith, M. and Valiullin, K.: "Stuck Pipe Prediction by Use of Automated Real-Time Modeling and Data Analysis," *SPE Drilling & Completion*, Vol. 32, Issue 3, September 2017, pp. 184-193.

4. Kucs, R.J.W., Spoerker, H.F., Thonhauser, G. and Zoellner, P.: "Automated Real-Time Hookload and Torque Monitoring," SPE paper 112565, presented at the IADC/SPE Drilling Conference, Orlando, Florida, March 4-6, 2008.

5. Mitchell, J.: *Trouble-Free Drilling: Stuck Pipe Prevention*, Drilbert Engineering Inc., 2001, 300 p.

6. Al Gharbi, S.H., Al Sanie, F.S. and Al Zayer, M.R.: "Automated Real Time Data Cleansing and Summarization: Case Study on Drilling Hook Load Real Time Data," SPE paper 176755, presented at the SPE Middle East Intelligent Oil and Gas Conference and Exhibition, Abu Dhabi, UAE, September 15-16, 2015.

7. Dunlop, J., Lesso, W., Aldred, W., Meehan, R., et al.: "System and Method for Rig State Detection," U.S. Patent No. 7,128,167, October 2006.

8. Nierdermayr, M., Pinckard, M.D. and Glaser, G.P.: "Automated Method and System for Determining the State of Well Operations and Performing Process Evaluation," U.S. Patent No. 6,892,812, May 2005.

9. Qahtan, A.A., Alharbi, B., Wang, S. and Zhang, X.: "A PCA-Based Change Detection Framework for Multidimensional Data Streams: Change Detection in Multidimensional Data Streams," *Proceedings of the 21st ACM SIGKDD International Conference on Knowledge Discovery and Data Mining*, August 2015, pp. 935-944.

About the Authors

Omogbolahan S. Ahmed

M.S. in Petroleum Engineering, Heriot-Watt University

Omogbolahan S. Ahmed is a Petroleum Engineer, working as Senior/Lead Real-Time Drilling Surveillance Engineer at Saudi Aramco's Real Time Operations Center (RTOC) in the Drilling Technical Department.

He started his oil and gas career at Shell Petroleum Development Company, Nigeria, where he worked as a Development Geologist between 2002 and 2008. Omogbolahan has more than 18 years of experience in the oil and gas industry.

Before joining Saudi Aramco in 2011, he worked as the RTOC Technical Coordinator for Futureware Company between 2008 and 2011.

Omogbolahan received his B.S. degree in Geology and Mineral Sciences from the University of Ilorin, Ilorin, Nigeria. He obtained a post graduate certificate in Petroleum Geosciences from the Shell Special Intensive Training Program for Graduates by Robert Gordon University, Aberdeen, Scotland.

Omogbolahan also received an M.S. degree in Petroleum Engineering from Heriot-Watt University, Edinburgh, Scotland. He is currently a Ph.D. candidate in the School of Energy and Chemical Engineering, Universiti Teknologi, Malaysia.

Omogbolahan is a Society of Petroleum Engineers (SPE) certified Petroleum Engineer.

Beshir M. Aman

M.S. in Applied Mathematics and Computational Science, King Abdullah University of Science and Technology

Beshir M. Aman has more than five years of experience as a Systems Analyst and a Project Lead working with Saudi Aramco's Drilling and Workover Systems Division, of the Petroleum Engineering Application Services Department. He is working on developing data science models that supports drilling engineers in the areas of drilling operation optimization, drilling trouble prediction, and drilling automation.

Beshir received his B.S. degree in Statistics from King Saud University, Riyadh, Saudi Arabia, and his M.S. degree in Applied Mathematics and Computational Science from King Abdullah University of Science and Technology, Thuwal, Saudi Arabia.

Dr. Majed A. Al-Zahrani

Ph.D. in Computer Science, King Abdullah University of Science and Technology

Dr. Majed A. Al-Zahrani is a Petroleum Engineering Systems Specialist working in Saudi Aramco's Drilling and Workover Systems Division, of the Petroleum Engineering Application Services Department. For the last 20 years, he has been the technical project manager of key strategic projects and solutions to support drilling engineers.

Majed has played a major and integral role in the development and delivery of many systems that introduced major business impact and led to optimizing and improving the day-to-day activities in Saudi Aramco's Drilling and Workover community.

He received his Ph.D. degree in Computer Science in the fields of machine learning and artificial intelligence from King Abdullah University of Science and Technology, Thuwal, Saudi Arabia.

Folorunsho I. Ajikobi

B.S. in Petroleum Geoscience and Drilling Engineering, Imperial College

Folorunsho I. Ajikobi is a General Supervisor of the Drilling Technical Department at Saudi Aramco. He joined Saudi Aramco in 2014, after gaining extensive experience working globally for various service companies and operators.

Folorunsho has participated in various Society of Petroleum Engineers (SPE) conferences and events as a steering committee member, speaker, and session chair.

He received his B.S. degree in Petroleum Geoscience and Drilling Engineering from Imperial College, London, U.K.

Clay Typing from Downhole Array Electromagnetic Measurements

Dr. Ping Zhang, Dr. Wael Abdallah, Dr. Shouxiang M. Ma, and Dr. Chengbing Liu

Abstract /

The amount and type of clays in reservoirs have a significant impact on formation evaluation and reservoir performance studies. Currently, clay typing requires either reservoir cores for laboratory analysis or advanced logs such as elemental spectral mineralogy (ESM) logs, both are available in only a small fraction of wells drilled. In this study, we will explore a possibility of using commonly measured logs to estimate clay volumes. Specifically, the logs used for the study are formation resistivity (RT), total formation porosity (PHIT), and gamma ray (GR). Since there are no known relationships relating these logs with clay volume, machine learning has been used for data analysis and parameter prediction. This is followed by exploring the possibilities of using array induction resistivity measurements to classify clay types downhole.

An important property of clay minerals is their ability to adsorb ions on their exposed surface, which is measured by its cation exchange capacity (CEC). We have developed a method of using induction resistivity data to extract CEC downhole, and display as depth profiles. There are four major types of clays commonly encountered in the oil fields: Kaolinite, chlorite, illite, and smectite, with their CEC values ranging from low to high.

Since each type of clay has its own CEC value, a synthetic CEC depth profile for any clay can be constructed if its volume fraction is known. On the other hand, CEC derived from the downhole resistivity data represents the combined effects of all the clay types presented in the formation being surveyed. By comparing the resistivity-based CEC profile with the synthetic ones, it is possible to define a volume fraction for each clay type, for the purpose of clay typing.

On the other hand, based on a previous developed method, total CEC representing the combined effects of all clays can be extracted from induction resistivity logs. By comparing the resistivity-based measured total CEC with the synthetic type curves, clay typing from downhole induction resistivity measurements is achieved. A workflow was developed for the application.

The proposed methodology was tested on the logs from six wells. The results indicated that RT, PHIT, and GR logs have strong correlations with clay volume and the model trained with these logs could be used to predict clay volumes for blind data sets. The workflow for clay typing was tested on the logs from two wells with positive results.

Introduction

Proper assessment of a reservoir requires accurate petrophysical evaluation of the reservoir. For example, any misinterpretation of porosity and saturation can have a larger impact on reservoir productivity and overall recovery. The presence of clay minerals are key factors affecting the proper evaluation of shaly reservoirs and the accurate determination of true reservoir saturation. Extensive studies regarding the effects of clays on the resistivity log response have been conducted over the past several decades[1-4]. It was found that the cation exchange capacity (CEC) values directly correlate with the clay type and content. Therefore, an accurate determination of formation CEC values is needed to properly estimate the water saturation.

A previous study demonstrated that the CEC values can be extracted from induction resistivity logs[5-7]. This work was primarily based on the theory of interfacial polarization commonly observed on clay grains coated by an electrical double layer and immersed in an electrolyte. The electrical double layer comprises the Stern layer and the diffuse layer. A complex conductivity was introduced to describe roles played by both layers. The in-phase and quadrature conductivities are strongly correlated with saturation and CEC values. By calculating in-phase and quadrature conductivities from the induction resistivity logs, both the saturation and CEC values can be estimated.

Clay in the rocks can affect different log readings. For example, the presence of hydrogen associated with the clay can greatly increase the apparent neutron log porosity, and therefore, the formation's total porosity (PHIT) as determined from the density neutron cross plot, if the clay effect is not corrected. Clay minerals can alter the formation resistivity (RT) such that a direct application of the Archie model yields an apparently high water

saturation. In addition, gamma ray (GR) logs are affected by the presence of clays.

Although the existence of clays affects all the above-mentioned noted logs, there are no established relationships linking RT, PHIT, and GR with clay volume. Therefore, machine learning techniques were evaluated to explore possible relationships. The logs from six wells were used to demonstrate the applications of the proposed methodology.

Elemental spectral mineralogy (ESM) logs from the same wells were used as references for the total clay volume. Then, a supervised machine learning technique — using an artificial neural network (ANN) — was performed, which demonstrated a clear correlation between the RT, PHIT, and GR with clay volume for the test data sets. The trained model was used to predict the clay volume for blind data sets.

For clay typing, a calculated CEC is a key input. The clay minerals most commonly encountered in reservoir rocks are kaolinite, chlorite, illite, and smectite, each having a well-defined CEC value. Subsequently, reservoir rock rarely contains only one type of clay, but typically has a mix of different clay minerals. Therefore, the goal of the clay typing in this study is to define a volume fraction for each clay mineral.

The CEC values calculated from resistivity logs and total clay volume estimated from the RT, PHIT, and GR logs are used to constrain and classify volume fraction for each clay mineral. With the help of a pattern recognition technique, the volume fraction for each clay mineral can be defined. A workflow was developed and tested on the logs from two wells with the final results comparing favorably with the ESM log answers.

Methodology

In this section, first, the details of how to extract CEC values from the induction resistivity logs are summarized. Then, methodologies of using machine learning techniques to explore possible correlations between the RT, PHIT, and GR logs with total clay volume are demonstrated. Finally, the calculated CEC values and total clay volume are used to define the volume fraction for each clay mineral.

Determine CEC Values from Resistivity Logs

The electrical property of a formation with clay inclusion is best described by a complex conductivity:

$$\sigma = \sigma^R + i\sigma^I \quad (1)$$

where σ^R and σ^I are the in-phase (R) and quadrature (X) components of the total formation conductivity, respectively[5].

Induction logs measure formation conductivity and are widely available in exploration and development wells. For clay-free formations, the calculated conductivity can be used to compute water saturations with the commonly used Archie's equation[8]; however, for a formation with clays, the interpretation process becomes much more complex.

An important property of clay minerals is their ability to attract ions on their exposed surfaces, primarily cations. This is a result of a net negative surface charge caused by their platy structure and by isomorphous substitution within the lattice frame. Clearly, this clay effect needs to be considered in formation evaluation. As extensions of Archie's equation, two commonly used shaly sand models are the Waxman-Smits model[1] and the dual water model[2], both incorporating a CEC parameter to account for the surface charges of clay minerals in a porous media.

In shaly sands, the application of an alternating electric field results in electric conduction (migration of charge carries) and interfacial polarization. The conduction current and interfacial polarization effects can be characterized by effective formation conductivity, σ_{eff}, and permittivity, ε_{eff}, which are calculated by measured R- and X- components from the resistivity log. Then, the in-phase and the quadrature conductivities can be calculated as:

$$\sigma^R = \sigma_{eff} \qquad \sigma^I = -\varepsilon_{eff} * 2\pi f \quad (2)$$

where f is the measurement frequency.

For a porous media containing clay minerals, the in-phase and quadrature conductivities can be expressed analytically[4] as:

$$\sigma^R = \frac{S_w^{n^*}}{F}\left[\sigma_w + \frac{2\, m^* \beta_+ \rho_g S_w^{-1} CEC}{3}(F-1)\right] \quad (3)$$

$$\sigma^I = -\frac{2}{3}\beta_+^s f \rho_g S_w^{n^*-1} CEC \quad (4)$$

where σ_w is the formation water conductivity, ρ_g is the grain density, F is the electric formation factor ($F = \phi^{-m^*}$), S_w is the water saturation, n^* and m^* are respectively the saturation and porosity exponents for a shaly formation, f is the fraction of counterion in the Stern layer, and β_+^s and β_+ are ion mobilities in the bulk fluid and Stern layer, respectively.

The conductivity model presented in Eqn. 3 and Eqn. 4 can be applied to field data to determine the in situ CEC and water saturation through inversion.

Estimating Clay Volume

The clay volume (V) is an important parameter for the evaluation of shaly formations. Total clay volume (V_T) is the sum of the kaolinite, chlorite, illite, and smectite fractions. Traditionally, the most convenient method for clay volume estimation is with GR logs, assuming a linear transform[9]. In many cases, such estimated clay volumes can be misleading, because minerals other than clay can also be radioactive.

One accurate way to acquire clay content is ESM concentration analysis through commercially available ESM logging tools. In this case, the tool measures a gamma spectrum, which are produced when high energy neutrons bombard the formation and lose energy through scattering, primary by hydrogen.

There is enough character in the measured spectrum to recognize the peaks caused by different elements. Through careful calibrations, these spectrum peaks can be related with elemental concentrations, which can be inverted to mineral groups, though ESM requires complex data processing algorithms.

In this study, the possibility of using commonly available log measurements to estimate clay volumes is explored. The logs employed are RT, PHIT, and GR. Each of these logs can be affected by the presence of clay minerals; however, there is no known relationship to evaluate the correlations between them. This is an ideal case for testing and applying machine learning techniques. The ANN is used to explore possible relationships between the RT, PHIT, and GR logs (predictors) with clay volume (target). More importantly, it will be very interesting to find out if the model defined by an ANN can be used for predictions on blind data sets.

ANNs are a common technique among the machine learning tools to analyze and solve complex problems, i.e., classification and regression. The concept of an ANN, which has found useful application in function regression, is an adaptation of the interconnection of brain neurons to a machine, for the nonlinear mapping of input to output[10]. The ANN architecture, consisting of an input layer, a hidden layer, activation function, and output layer, controls how the nonlinear mapping of input to output works. The nonlinear mapping of the predictors and target is established by training the ANN. This step is considered an optimization problem with an objective function defined by the standard least-squares method.

The data sets used for this study were obtained from six wells located in different oil fields. Table 1 lists the detailed information regarding the logs and data points for the six wells. The processed logs — RT, PHIT, and GR — were selected as predictors. ESM measurements from the same wells are used to estimate clay volumes, which are used as targets for supervised machine training. Figure 1 shows an example of a data set used for the training process. To ensure consistency among the logs, a normalization is applied to all the logs to ensure the data values are within the range of -1 and +1:

$$X_n = \frac{2*X - X_{max} - X_{min}}{X_{max} - X_{min}} \quad (5)$$

Table 1 *Well data used for machine learning.*

Well Code	Number of Data Points	Oil Field	Data Used for Machine Learning
Well-1	551	A	RT, PHIT, GR
Well-2	2,551	A	RT, PHIT, GR
Well-3	1,251	A	RT, PHIT, GR
Well-4	1,301	B	RT, PHIT, GR
Well-5	1,301	C	RT, PHIT, GR
Well-6	1,501	C	RT, PHIT, GR

Fig. 1 *The processed logs used for model training. Data are normalized to within a range of -1 and +1.*

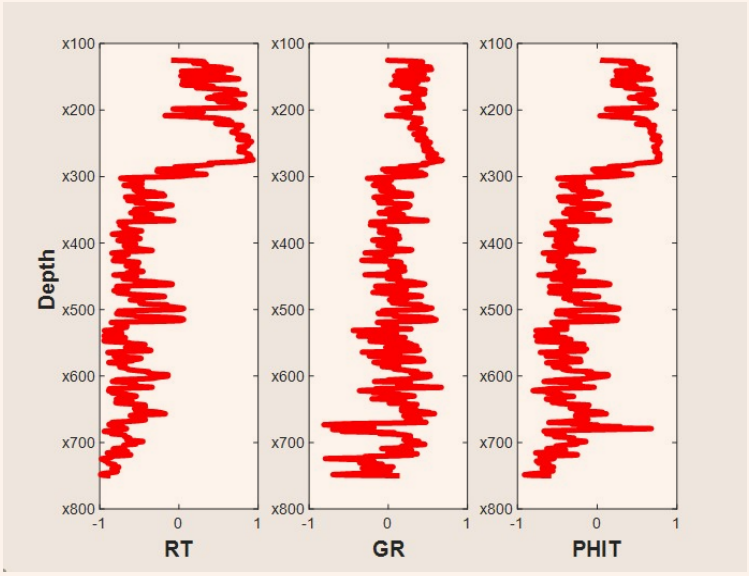

where X_n, X, X_{max}, and X_{min} denote normalized, actual, maximum, and minimum data, respectively.

The optimum ANN parameters to realize the best performance are evaluated with two statistic parameters; the coefficient of correlation (R), and the mean square error (MSE):

$$R = \frac{Covariance(X_{measured}, X_{predicted})}{standard\ deviation(X_{measured}) \times standard\ deviation(X_{predicted})} \quad 6$$

$$MSE = \frac{1}{n}\sum_1^n \left(X_{measured} - X_{predicted}\right)^2 \quad 7$$

Regression R values measure the correlation between the model outputs and targets. An R value of 1 means a perfect correlation, 0 is a random relationship. MSE is the average squared difference between the outputs and targets. Lower values are better. Zero means perfect predications, no errors.

To investigate the impact of the predictors on the clay volume (target), the relevancy factor (fr) is defined as follows[11]:

$$fr(Inp_k, X_{pre}) = \frac{\sum_{j=1}^n (Inp_{k,j} - Inp_{ave,k}) \times (X_{pre,j} - X_{ave})}{\sqrt{\sum_{j=1}^n (Inp_{k,j} - Inp_{ave,k})^2 \times \sum_{j=1}^n (X_{pre,j} - X_{ave})^2}} \quad 8$$

where X_{pre} denotes the output values of the trained model and X_{ave} represents the average output values, index k represents the RT, PHIT, and GR. $Inp_{k,j}$ is the j^{th} value of the k^{th} input and $Inp_{avg,k}$ is the average value of the k^{th} input. A larger value of fr between a predictor and output indicates that the output is highly dependent on the predictor.

The ANN model trained with the above-mentioned data sets was built using the MATLAB computing platform. The normalized data were then randomized and segregated into a partition of training (70%), validation (15%), and testing (15%). Data randomization was done to ensure fair representation of the data sets in the training, validation, and testing partition.

This step is considered an optimization problem with an object function defined by the standard least-square method. To minimize the object function, the weights for all the neurons are updated based on the Levenberg-Marquardt backpropagation. The validation of the data was performed to ensure that the model did not over fit the data. The final assessments of the model's performance were represented by R and MSE.

Estimating Volume Fraction for Each Clay

Clay minerals may be grouped, on the base of molecular structure and composition, into the four most commonly encountered and representative groups: kaolinite, illite, chlorite, and smectite. Although each clay group impacts formation conductivity differently, the fundamental mechanism is similar. Each clay type has different characteristics, which is mostly translated to its CEC. For a formation rock containing mixed clay minerals, the apparent CEC can be calculated based on the below mixing law:

$$CEC = W_C \times CEC_C + W_I \times CEC_I + W_K \times CEC_K + W_S \times CEC_S \quad 9$$

$$W_T = W_C + W_I + W_K + W_S \quad 10$$

where W_T is the total clay weight fraction, and W_C, W_I, W_K, and W_S are the clay weight fractions for chlorite, illite, kaolinite, and smectite, respectively. CEC_C, CEC_I, CEC_K, and CEC_S are the CEC values for chlorite, illite, kaolinite, and smectite, respectively. The CEC value for each above-mentioned clay mineral is well-defined and can be treated as a known parameter. The clay volume can be calculated from the clay weight using the following formula:

$$V_{cl} = \frac{\rho_{matrix}(1 - \phi_{total}) \times W_{cl}}{\rho_{cl}} \quad 11$$

where ϕ_{total} is the formation's total porosity, ρ_{matrix} is the matrix density, and ρ_{cl} is the density of the clay. From the previous sections, the apparent CEC can be defined from resistivity logs and the total clay volume can be predicted from the RT, PHIT, and GR logs.

The volume fraction of each clay type, on the other hand, is unknown and needs to be determined for clay typing. Therefore, there are four unknowns (V_C, V_I, V_K, V_S) in Eqns. 9, 10, and 11, which do not have a unique solution. A possible way to solve this problem is to use pattern recognition. We pre-assume a volume range for each clay mineral, and allow a small volume incremental within the range. As a result, there are many volume selections for each clay mineral. For all four clay minerals, there are a large number of possible combinations of the volume fractions. Consequently, not all of the combinations are valid as they must satisfy the constraint of Eqn. 10. For those valid volume combinations, apparent CEC values can be calculated using Eqn. 9, resulting in many CEC depth profiles. Then, these CEC depth profiles are compared against the one calculated from the resistivity log — ground truth. An optimal CEC profile is defined as the one closest to the ground truth, and the volume fraction of each clay mineral is also determined. The entire workflow is presented in Fig. 2.

Fig. 2 *Workflow defining the volume fraction for each clay mineral.*

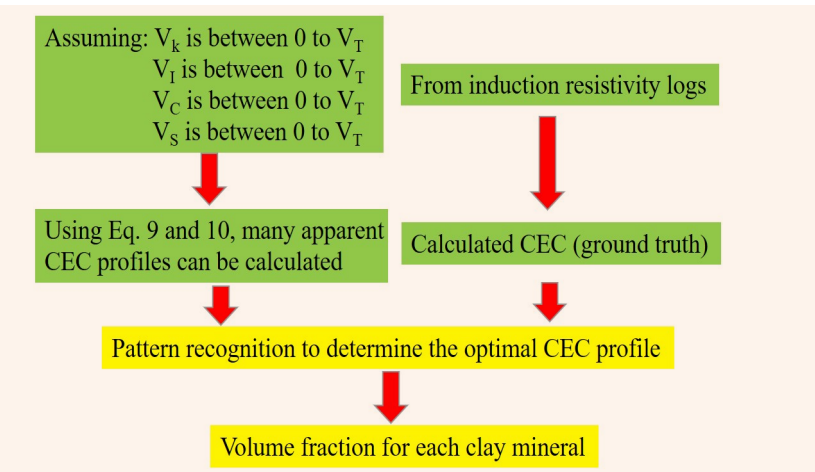

Results and Discussion

A total of 8,456 data points from six wells were pre-processed and trained using ANN. The training process was repeated many times with different parameter settings to ensure the optimal model was defined. To analyze the training performance, a group of post-processing plots are generated. The first plot is the error histogram, Fig. 3, which shows the difference between the targets and the predicted outputs. The error has Gaussian distribution with a zero mean. There are no obvious biased errors in the training, validation, and test process. The cross plots of the predictions for training and testing are presented in Fig. 4. It seems that the relationship and degree of association between the predicted clay volume (from RT, PHIT, and GR) and the true clay volume (from ESM) are very good (R = 0.98), Fig. 4a. Similarly, a high correlation (R = 0.97) is observed for the testing data, Fig. 4b. This would suggest that the RT, PHIT, and GR logs are good predictors, and that the model trained based on these logs should be able to predict the clay volume with high accuracy. This observation is further confirmed with the plot in Fig. 5, which shows the data fit between the predicted outputs (black), and the targets (red). The majority of data points fit very well, with a few outliers near the end of the data records. The mean square error is very small: 0.015. To understand the relative importance of each predictor, the *fr* defined in Eqn. 8 is plotted in Fig. 6. It can be concluded that the porosity has the greatest impact on the clay volume, and the GR has the second greatest impact, followed by resistivity.

Fig. 3 *Error histogram for training, validation, and testing.*

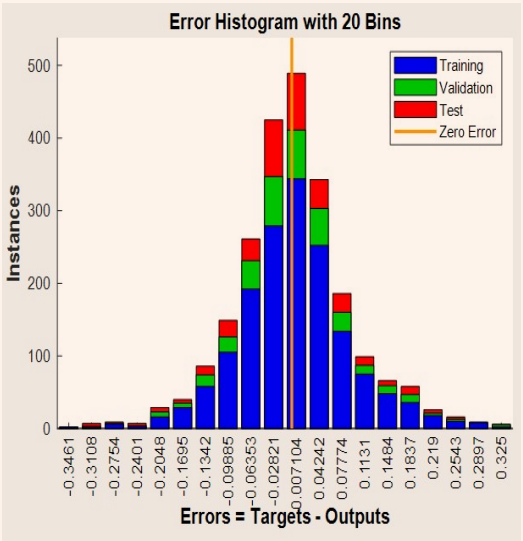

The model training appears very successful, as evidenced by all the post-processing plots. The next step is to investigate if the successful model training can be translated into a predicting power. A blind test was processed as follows:

- The model was re-trained with logs from only five wells (Well-2 was dropped).
- The trained model was applied on the RT, PHIT, and GR logs from Well-2 to predict clay volume.
- The predicted clay volume was compared with that from the ESM.

The results are presented in Figs. 7a and 7b. As expected, both the correlation coefficient (R = 0.95) and the data misfits (MSE = 0.05) are worse than the ones when all the data were included. Subsequently, considering that for this model training logs from Well-2 were never used, and the remaining five wells are from different fields, the results are considered acceptable. This model training exercise demonstrates that the RT, PHIT, and GR have good correlations with the clay volume. Since

Fig. 4 *The prediction of the training data (a), and the prediction of the testing data (b).*

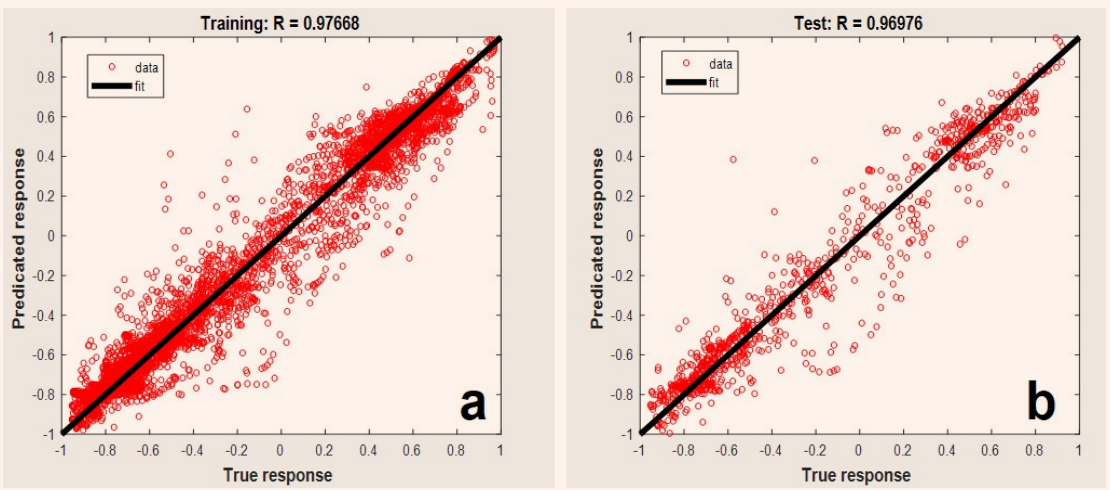

Fig. 5 *Data fit between the predicted outputs (black), and the targets (red).*

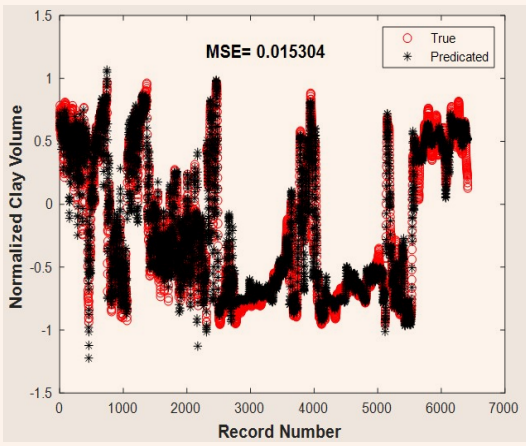

Fig. 6 *The relevancy factor (fr) of each predictor.*

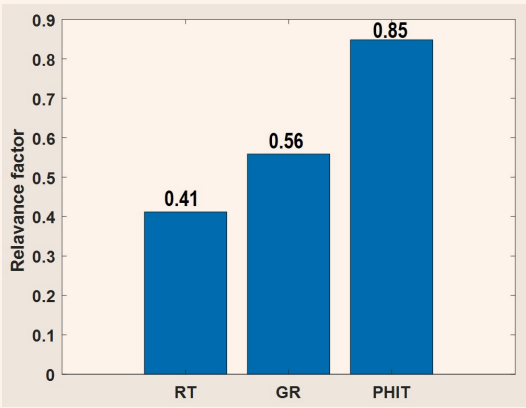

all of these logs are routinely acquired in oil fields, the proposed method has the potential for development into a practical application for clay volume evaluation.

Each oil field has its own unique geological structure and conditions. The ANN model presented here is trained with the data from the fields with similar geological structures. For other fields, the model should be trained with local logs. The fundamental difference between a deterministic model and an ANN model is that the former can be applied to practically any oil field, but the latter must be trained for each field using local data.

The clay typing is processed according to the workflow presented in Fig. 2. Resistivity logs from two wells are selected to test the workflow. The downhole CEC profile was calculated from the resistivity data and used as a constraint for Eqn. 9. The total clay volume predicted using the ANN is used to constrain Eqn. 10. As a result, the volume fraction for each clay mineral in these two wells is estimated based on pattern recognition. To validate the results, the volume fraction from the ESM logs is used as a benchmark.

Figure 8 shows the results from the first well. There are three different clay minerals in this well: illite, chlorite, and kaolinite. The black line shows the volume factions based on the ESM log, and the red line denotes the clay volume fractions calculated using the workflow. While the overall agreement is good, there are some discrepancies between the two estimations. This is especially true for chlorite, as the estimation based on the workflow is systematically higher than the one from the ESM.

There are only two clay minerals in the second well: illite and chlorite. The results are presented in Fig. 9. The two estimations have excellent agreements over the entire depth section. The clay typing works very well for this well. The overall results from these two test wells are very encouraging, considering that the method based on the workflow is very much different from the one based on the ESM. It demonstrates that the proposed workflow

Fig. 7 *The prediction of the training data (a), and the data fit between the predicted outputs (black) and targets (red) (b).*

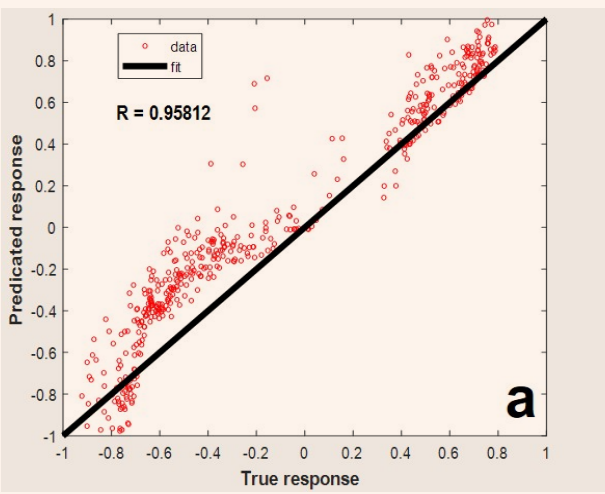

can provide qualitative, even quantitative, analysis about clay content. Furthermore, since the resistivity log is widely available, this clay typing method may provide an alternative and simple application for clay identification.

Conclusions

The primary purpose of this study is to find a practical way for clay typing using commonly available logs. The process includes two parts:

1. Estimate the total clay volume from the RT, PHIT, and GR logs.
2. Identify each clay type and estimate its volume fraction.

The first task was accomplished using machine learning

Fig. 8 *A comparison of the clay typing results between the ESM (black) and the workflow (red) for Well-1.*

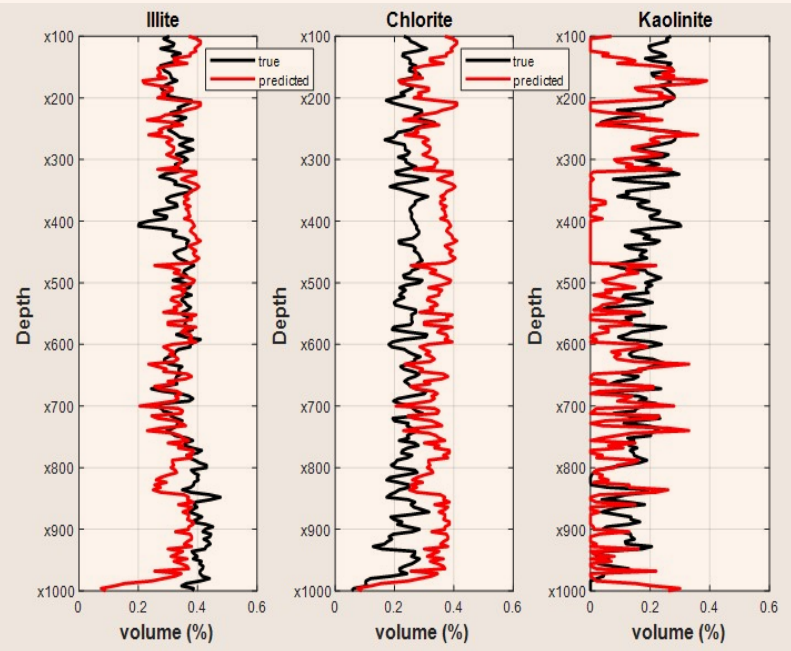

Fig. 9 *A comparison of the clay typing results between the ESM (black) and the workflow (red) for Well-2.*

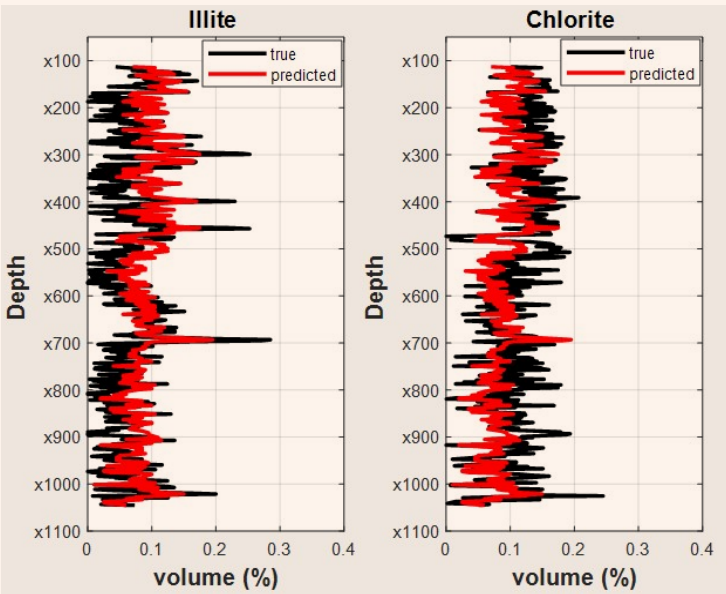

techniques. An ANN was successfully used to train a model, which can be used to predict the clay volume with good accuracy.

The second task is only possible based on our previous work of using the resistivity logs to estimate the in situ CEC values. A workflow was developed to estimate the volume faction for each clay mineral, based on the calculated CEC and total clay volume. Logs from two wells were tested with generally positive results.

Although there are errors and uncertainty with the proposed workflow, it does have the potential to become a useful method for clay typing, qualitatively, or semi-quantitatively.

Acknowledgments

This article was presented at the 2020 International Petroleum Technology Conference, Dhahran, Saudi Arabia, January 13-15, 2020.

References

1. Waxman, M.H. and Smits, L.J.M.: "Electrical Conductivities in Oil-Bearing Shaly Sands," *Society of Petroleum Engineers Journal*, Vol. 8, Issue 2, June 1968, pp. 107-122.
2. Clavier, C., Coates, G. and Dumanoir, J.: "Theoretical and Experimental Bases for the Dual Water Model for the Interpretation of Shaly Sands," *Society of Petroleum Engineers Journal*, Vol. 24, Issue 2, April 1984, pp. 153-168.
3. Revil, A., Cathles III, L.M., Losh, S. and Nunn, J.A.: "Electrical Conductivity in Shaly Sands with Geophysical Applications," *Journal of Geophysical Research*, Vol. 103, Issue B10, October 1998, pp. 23925-23936.
4. Revil, A.: "Spectral Induced Polarization of Shaly Sands: Influence of the Electrical Double Layer," *Water Resources Research*, Vol. 48, Issue 2, February 2012.
5. Zhang, P., Abdallah, W., Ma, S.M., and Liu, C.: "Extracting Rock Cation Exchange Capacity from Electromagnetic Measurements," paper presented at the SPWLA 59th Annual Logging Symposium, London, U.K., June 2-6, 2018.
6. Wang, G.L., Homan, D.M., Uschner-Arroyo, N., Zhang, P., et al.: "Determining Resistivity and Low-Frequency Dielectric Constant Using Induction Data in the Presence of Strong Induced Polarization," paper presented at the SPWLA 60th Annual Logging Symposium, The Woodlands, Texas, June 15-19, 2019.
7. Ma, S., Zhang, P. and Abdallah, W.: "Cation Exchange Capacity and Water Saturation from Array Induction Data," U.S. Patent 10,215,876, February 26, 2019.
8. Archie, G.E.: "The Electrical Resistivity Log as an Aid in Determining Some Reservoir Characteristics," *Transactions of the AIME*, Vol. 146, Issue 1, December 1942, pp. 54-62.
9. Heslop, A.: "Gamma Ray Log Response of Shaly Sandstones," paper presented at the SPWLA 15th Annual Logging Symposium, McAllen, Texas, June 2-5, 1974.
10. Wythoff, B.J.: "Backpropagation Neural Networks: A Tutorial," *Chemometrics and Intelligent Laboratory Systems*, Vol. 18, Issue 2, February 1993, pp. 115-155.
11. Chen, G., Fu, K., Liang, Z., Sema, T., et al.: "The Genetic Algorithm-Based Back Propagation Neural Network for MMP Prediction in CO_2 EOR Process," *Fuel*, Vol. 126, June 2014, pp. 202-212.

About the Authors

Dr. Ping Zhang

Ph.D. in Geophysics, Uppsala University

Dr. Ping Zhang started his career as a Researcher at the University of Montreal, Montreal, Canada, from 1990 to 1994 and an Area Geophysicist for Inco Ltd., a mining company in Canada from 1995 to 1998. He joined Schlumberger in 1999 and is currently a Principal Geophysicist. Ping's research has focused on the applications of electromagnetic (EM) technology for geophysical exploration and formation characterization, with emphasis on developing numerical techniques for interpretation of EM data.

He was a principal developer for cross-well EM technology and worked on data processing, inversion and interpretation for petroleum applications. Recently, Ping has been actively involved in studies of using downhole EM logs for cation exchange capacity determination and clay typing. In addition, he is also actively engaged in a research effort of using low frequency permittivity for estimating saturation in freshwater and mixed salinity environments.

Ping has published more than 50 peer-reviewed conference papers and holds 12 granted U.S. patents. He is a member of the Society of Petroleum Engineers (SPE), the Society of Petrophysicists and Well Log Analysts, and the Society of Exploration Geophysicists.

In 1989, Ping received his Ph.D. degree in Geophysics from Uppsala University, Uppsala, Sweden.

Dr. Wael Abdallah

Ph.D. in Chemical Engineering, University of Alberta

Dr. Wael Abdallah joined Schlumberger in 2005 as a Research Scientist at the DBR Technology Center, Edmonton, Canada. He is currently the Managing Director of Schlumberger's Dhahran Carbonate Research Center in Saudi Arabia.

Prior to this assignment, Wael was the Program Manager for the rock physics and recovery research activities within the same center. He also managed commercial services related to reservoir fluids phase behavior and flow assurance. Wael also worked as an instructor with the NeXT technical training team on reservoir fluids.

In 2005, he received the Alberta Ingenuity Award.

Wael has published and coauthored more than 70 peer-reviewed conference papers, in addition to having 15 granted U.S. patents.

He is a member of the Society of Petroleum Engineers (SPE) and the Society of Petrophysicists and Well Log Analysts. Wael holds a professional Engineering Status in Canada.

He received both his B.S. and M.S. degrees in Chemical Engineering from the Jordan University of Science and Technology, Irbid, Jordan, majoring in fluid phase behavior and thermodynamics.

In 2005, Wael received his Ph.D. degree in Chemical Engineering from the University of Alberta, Edmonton, Canada, majoring in heterogeneous catalysis and surface science.

Dr. Shouxiang M. Ma

Ph.D. in Petroleum Engineering, New Mexico Institute of Mining and Technology

Dr. Shouxiang M. "Mark" Ma is a Senior Consultant overseeing research and development, subject matter technical support, and professional development in the Advanced Petrophysical Modeling Group of Saudi Aramco's Reservoir Description and Simulation Department. Prior to this, he was Supervisor of the Petrophysical Support & Study Unit, advisor at the Upstream Professional Development Center, and Lead Petrophysicist for logging operations.

Before joining Saudi Aramco in 2000, Mark worked at the Exxon Production Research Company, Wyoming Western Research Institute, New Mexico Petroleum Recovery Research Center, and China Yangtze University.

He served as a chairperson of the 2013 Society of Petroleum Engineers (SPE) Formation Evaluation Award Committee, the 2018 SPE Annual Technical Conference and Exhibition Formation Evaluation Committee, and the 2019 International Petroleum Technology Conference Education Week.

Mark was awarded the 2019 SPE MENA Formation Evaluation Award.

He currently serves on the *JPT* Editorial Board and the Society of Petrophysicists and Well Log Analysts (SPWLA) Board of Directors for the Middle East and Africa area. Mark is also an Associate Editor for the *Journal of Petrophysics*, and Vice President of the SPWLA Saudi Arabia Chapter.

He received his B.S. degree from the China University of Petroleum, Shandong, China, and his M.S. and Ph.D. degrees from the New Mexico Institute of Mining and Technology, Socorro, NM, all in Petroleum Engineering.

Dr. Chengbing Liu

Ph.D. in Geology, Geology Institute of Chinese Academy of Science

Dr. Chengbing "CB" Liu is a Petrophysics Consultant working in the Advanced Petrophysical Modeling Group of Saudi Aramco's Reservoir Description and Simulation Department. His current technical focus is low resistivity/low resistivity contrast pay identification, new applications of electrical/di-electrical logging via integrating with nuclear magnetic resonance (NMR)/wireline formation test, and horizontal well log interpretation.

Before joining Saudi Aramco, CB worked for Chevron for 10 years as a Sr. Staff Petrophysicist at ETC/USA, Lead Petrophysicist at MCBU/USA, and Petrophysics Team Leader at PZ/Kuwait. Before Chevron, he worked for Schlumberger for 14 years as GeoCenter Manager at DCS-Beijing/China, Sr. R&D Petrophysics Specialist at the LWD Resistivity and NMR Department of SPC/USA, and Petrophysics Discipline Leader at DCS-KL/Malaysia. Prior to this, CB worked for CNPC for a few years, first as a Field Engineer and then as the Director of the FE Department at SOLC/China.

He is an Associate Editor for the *Journal of Petrophysics*. CB has published two books and 25 papers. He holds 12 U.S. granted patents.

CB received his B.S. degree in Petrophysics from the China Petroleum University, Beijing, China, and his Ph.D. degree in Geology from the Geology Institute of Chinese Academy of Science, Beijing, China.

Using "Digital Twin" of Coriolis Meters for Multiphase Flow Measurement

Dr. Sakethraman Mahalingam and Dr. Muhammad Arsalan

Abstract /

Multiphase flow meters are often built based on one or many single-phase flow metering technologies. Following the trend, Coriolis meters are being increasingly used in upstream applications in conjunction with an independent water cut meter to measure multiphase flow. Coriolis meters are well-known for fiscal metering applications as they offer unparalleled accuracy without having to input detailed information on the fluid being metered. They offer two distinct measurements: (1) density, and (2) mass flow rate, which is often not possible with other metering technologies. Subsequently, under multiphase flow, the biggest problem with liquid Coriolis meters is their tendency to stall when large amounts of gas flows through them.

Many manufacturers over the last 10 years have developed techniques to adjust the drive gain to enhance the ability of these meters to handle increasing amounts of gas. There have also been several developments in using advanced signal processing and machine learning methods to help the meters to self-calibrate and correct for the presence of gas. These methods range from a simple error analysis on certain raw measurements to more sophisticated "digital twin" based concepts to simulate the behavior of the Coriolis meter internally.

This article describes the concept of digital twin in detail and outlines the reasons for the superiority of such an approach.

Introduction

Coriolis meters are used extensively in downstream oil and gas applications, such as fiscal metering, because the technology offers measurement uncertainties that are fractions of 1%. In addition, the meters provide two measurements: (1) density, and (2) mass flow rate, and work without much information on the metered fluids, right out of the box. As with other single-phase meters, Coriolis meters are being increasingly used in upstream applications, where instead of being a single fluid, the metered fluid is a mixture of oil, water, and gas.

One of the popular uses of Coriolis meters is to infer the water fraction at the output of a separator where the density measurement on the meter is translated into a water cut. This application is accomplished as there is very little gas in the flow line. The technology has also been coupled with an independent water cut meter for full multiphase measurements[1]. Consequently, Coriolis meters suffer from two main issues under multiphase flow: (1) an inability to maintain tube vibrations safely, and (2) even if vibrations were kept up, there are big errors in the measurement caused by the decoupling and compressibility of the gas phase[2]. The first issue has been largely addressed with digital drive Coriolis meters[3-5].

Multiphase meters are built combining several metering technologies, and consequently, suffer from the disadvantages of the constituent technologies. In fact, there are three main reasons why multiphase metering provides almost the perfect use case for using data analytics techniques, especially digital twins.

First, there is a wealth of data from the set of sensors within the multiphase meter, and physics is only able to explain some of the data. Second, while offline analysis of meter data often shows value in data analytics, the computing power of the meters themselves are limited to utilize these techniques in real-time. In particular, the digital twin technology enables the use of the toolkit used in the design of the meter in the interpretation of live measurements. It may not be possible to integrate these tools into the meter, even if the computing power of the meter was improved. Third, since the meter is often one of the sources of measurements for the operators, the operator would be able to use data from the rest of the upstream infrastructure to build a complete model of the well, field, and/or reservoir to achieve better allocation and reservoir management.

Coriolis Meters under Multiphase Flow

Within the Coriolis meter, the flow is often split into a pair of customized flow tubes, and the two tubes are vibrated at frequencies in the order of a few hundred Hz. There are two pickups, one at each end of the meter, that measure the movement of the tubes continuously, Fig. 1[6-8]. The resonant frequency of the tubes is altered due to the presence of fluids within the tubes, and this relationship is used to measure the density of the fluid. The flow

Fig. 1 *Coriolis meter[7-9].*

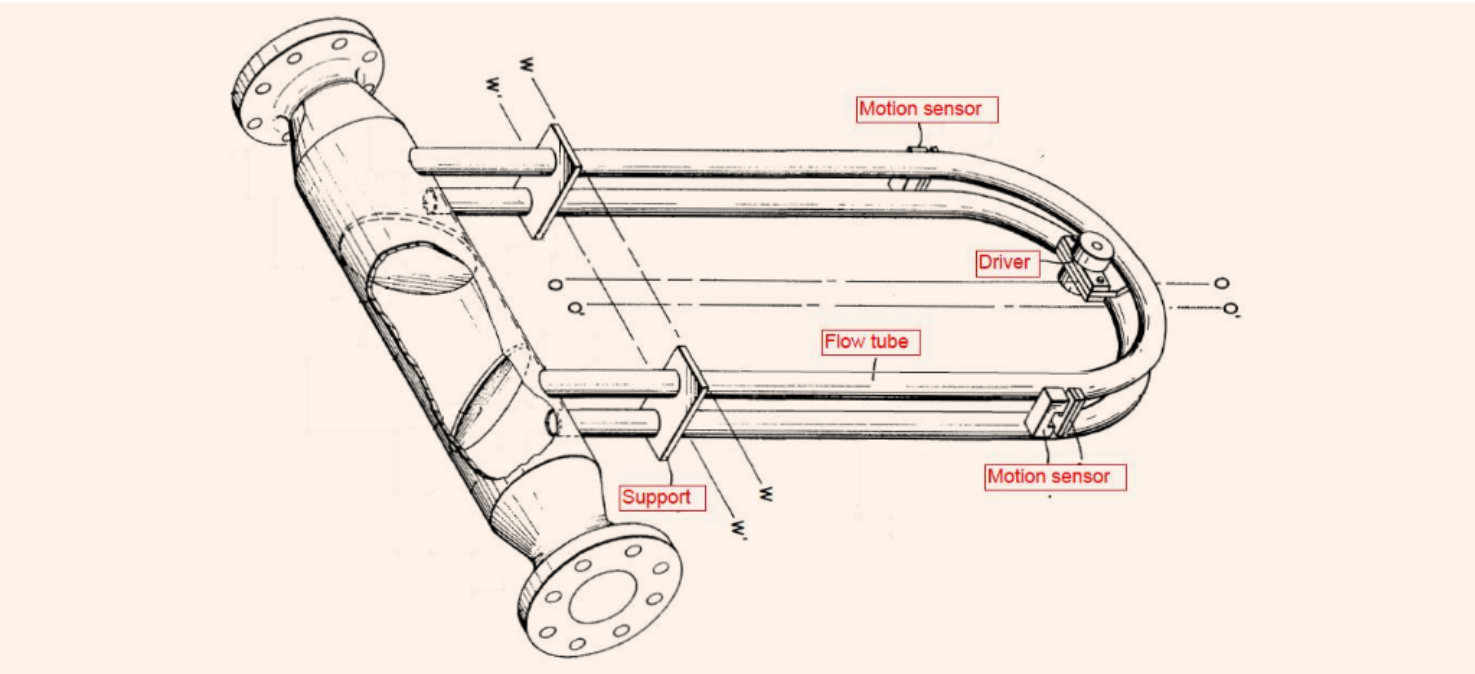

of fluid causes an additional out-of-plane twist in the tubes due to the Coriolis Effect. This results in a phase shift between the two pickups and is used to measure the mass flow rate of the fluid.

Under multiphase flow, specifically when liquids and gas are flowing together, the center of mass of the fluid within the tubes and the center of mass of the tubes themselves are no longer coincident. This is one of the assumptions built into the calibration of the meter, and any deviation from this assumption causes errors in the measured density and mass flow rate. There are two main issues with entrained gas flowing through Coriolis meters: (1) gas compressibility, and (2) phase decoupling[2, 9]. Given that the gas is compressible, the movement of the tubes can cause them to be squeezed against the trailing wall of the vibrating tube, Fig. 2.

In extreme situations, a transverse acoustic mode of vibration may be introduced — like a flexible hose shaking as entrained gas comes out of the hose when connected to the water tap. In this situation, the gas is traveling back and forth within the tube walls and causes the hose to shake. The frequency of the vibration imposed on the tubes is often close to the natural frequency of the tube itself, and in any case, this must be far away from the frequency of such transverse acoustic modes as they can lead to unsafe resonances in the system.

While the liquid may follow the tube in its motion, the gas tends to decouple and stay suspended within the liquid, causing them to decouple from the tube vibrations. The viscosity of the fluid affects the "coupling" between the tube and fluid. Higher viscosities are better because the fluid tends to follow the vibration induced on the tube closely, leading to less errors. A higher viscosity liquid keeps the lighter gas moving in synchronization with the tube. Moreover, higher viscosities may cause larger pressure drops across the Coriolis meter, which may not be desirable[10]. Given that the viscosity of gas is much lower than the liquid, it tends to decouple from the induced vibration on the tube. The error caused by the decoupling of the gas phase is lower for liquids with a higher viscosity[2, 9, 11].

In terms of operation, a Coriolis meter used for metering gas operates at a different frequency, power, and measurement sensitivity, when compared to one used for metering liquids. To make the Coriolis meter capable

Fig. 2 *A diagram showing the reaction of the gas due to movement of the tubes: (a) gas compressibility, and (b) decoupling.*

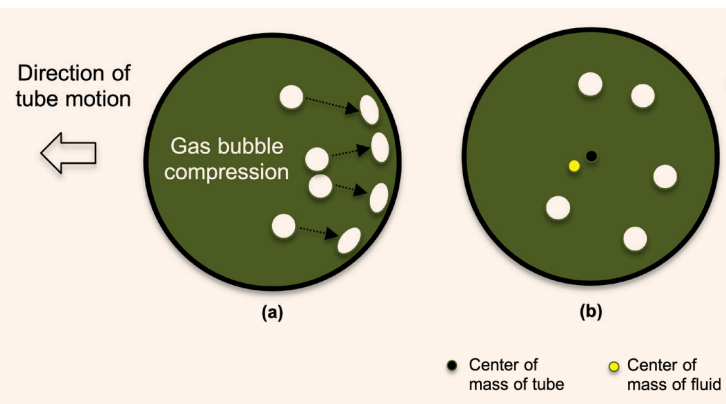

of metering multiphase flow, the meter must be able to sustain vibrations and make valid measurements of frequency and phase shift in the presence of gas, which causes increased damping. Gas compression and decoupling increases energy dissipation due to damping[1, 12], and to keep the vibrations going, more energy must be put into driving the meter — this is often referred to as "drive gain"[13].

If the Coriolis meter can maintain tube vibrations and make valid measurements in the presence of gas, the Coriolis meters may be "recalibrated" by testing them extensively under multiphase flow. An analytical framework to analyze the errors in a Coriolis meter with entrained gas is described in Hemp and Kutin (1999)[9]. According to this data, the errors in density and mass flow rate for zero viscosity liquid aerated with zero density gas are given by Eqns. 1 and 2. An interesting insight is that the errors in a highly viscous liquid with entrained gas is lower than in a less viscous liquid.

$$E_d = -3\alpha + \frac{1}{4}\left[\frac{w_1 b}{c}\right]^2 \quad (1)$$

$$E_{\dot{m}} = \frac{-2\alpha}{1-\alpha} + \frac{1}{2}\left[\frac{w_1 b}{c}\right]^2 \quad (2)$$

where E_d = error in density, a = gas volume fraction, w_1 = actual resonance frequency of vibration for a two-phase fluid, b = inner diameter of the flow tube, and c = speed of sound in a two-phase fluid.

While experiments have been shown to follow the trend given by Eqns. 1 and 2, there is not a 100% agreement. Under these circumstances, using the theoretical error model as a basis, a neural network model may be used to pick up patterns in the data that cannot be fully explained by physics[14].

In the field, the guidance given by manufacturers in terms of orientation, entry and exit conditions are often not fully followed, due to practical considerations in the field. There is an effect of such deviations and it is almost impossible to run calibration tests under every possible circumstance encountered in the field.

Meter Diagnostics and Health Monitoring

Two developments for Coriolis meter diagnostics are already available from manufacturers: (1) entrained gas handling, and (2) tube health monitoring. Many manufacturers seem to offer at least one of the two features. The entrained gas handling from Emerson Micro Motion[12] relies on using the drive gain as an indicator of the presence of gas. This is then extended to use the last known liquid density (when the drive gain was low) to correct for the measurements when the gas is present. This is an example of self-calibration and the meter adapting to the flow. Endress + Hauser have developed a dual frequency Coriolis meter, which claims to handle entrained gas better than before[15].

The health monitoring of the Coriolis meter tubes is also an important feature. A meter operated at 100 Hz may undergo over 8 million cycles in a day, albeit at very low stress levels. In addition, corrosion, erosion, scaling, and fouling are all possible when meters are used in upstream conditions, and therefore, it is important to know the health of the flow tubes. Any change in the mechanical structure of the meters causes not only errors, but also has implications for safety.

Digital Twin Approach

The term "digital twin" has a wide range of meanings where anything, from a prognostics based on a coupled finite element model[16], to the virtual simulation of an aircraft engine. Definitions of digital twin from Grieves and Vickers (2016)[17], Glaessgen and Stargel (2012)[18], and Fei et al. (2019)[19] give us the three key ingredients: (1) the real device, (2) the virtual device, and (3) the connection between the two. The connection between the real and virtual meter is the most important part of this approach. Without that, most "offline" diagnostics used today may be classified as digital twin. In these cases, the direction of data travel is one-way, from the meter to the offline model. Certain outcomes are diagnosed using the model and in case of prognostics, a future path is predicted.

It is important to emphasize that the connection between the real and virtual device enables the real device to alter its operation autonomously or semi-autonomously, based on the feedback received from its digital twin and vice versa, Fig. 3. In a sense, the self-calibration of the Coriolis meter is one of the simplest examples of such a change in operation — the meter deviates from its factory calibration progressively based on actual measurements in the field. Consequently, this may be based on a simple routine embedded within the flow meter itself without much consideration for all the measurements. A digital twin is a much more comprehensive digital description of the device and a decision to self-calibrate may be arrived at by using many more measurements that are processed through a comprehensive model of the device.

The digital twin may run at the flow meter or in the cloud depending upon the computing resources, and the speed at which operations may have to be altered in the real device. The digital twin approach must enable data going the other direction as well, so that the digital twin may be altered. For example, erosion of the flow tubes in the Coriolis meters may be measured either directly or indirectly in the real device, and this information may be used to alter the digital twin to correspond more closely with the real device in the field. The digital twin may then compute that the calibration of the meter needs to be altered, and thereby communicate this to the real device. The meter may now be operated in a different mode.

Installation conditions have a big effect on the flow meter's performance, but are often ignored. For example, on a horizontal flow line, Coriolis meters must not be installed in an "inverted U" position in liquid flow, as even a small amount of gas in the meter can be locked within the meter. The best position for a gas Coriolis meter is for them to be installed in the "inverted U" position, as any liquid is the flow would naturally fall out of the meter due to gravity. Multiphase flow meters are recommended to be installed in the vertically upward flow, just after a blind-T junction to ensure homogeneity of the flow. In other cases, there may be specifications that require a certain amount of straight pipe run before

Fig. 3 *The digital twin approach to flow metering.*

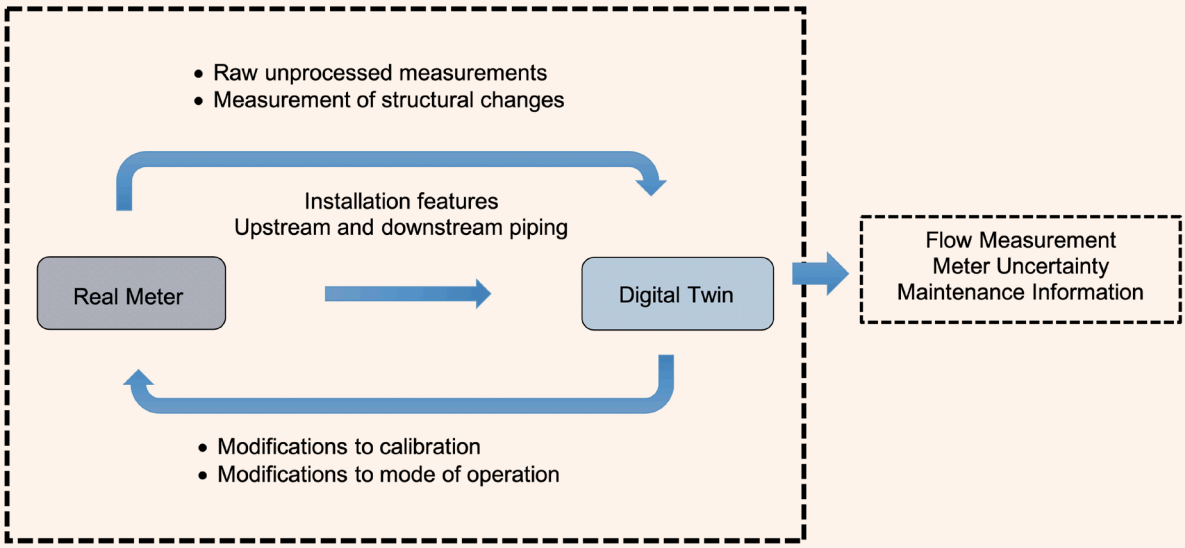

and/or after the meter, though such requirements are almost never followed in real life. There are innumerable scientific studies conducted on the installation effects of standard flow meters like Venturi meters[20]. The learning from such studies is not used extensively in multiphase flow meters.

The digital twin approach can enable the operator to capture installation conditions precisely. The digital twin can include parts of the upstream and downstream pipework and the orientation of the meter in the field. The effect of multiphase flow on the meter can be more closely modeled, and corrections to the measurements may be provided.

A radical digital twin approach would be to design the meter with a lot more flexibility in terms of gas handling with potentially other sensors integrated into the meter to measure pressure before and after the meter. This would mean that the meter would tune itself to the process condition, and then have the possibility of receiving additional input from a virtual or physical meter elsewhere in the system.

Coriolis Meter "Twin" Modeling

The Coriolis meter calculates and reports the density and mass flow rate as two independent measurements. The two main measurements within the meter that correspond to the reported measurements are the frequency and phase shift between the entry and exit pickups, respectively. Subsequently, there are other measurements that have an indirect effect on the meter, such as the temperature and the drive power needed to sustain the vibrations.

These may not qualify to be "truly" independent measurements, but are nevertheless useful in diagnosing the meter and its performance. There are several parameters that are typically logged in a Coriolis meter[13]. Of course, these are used indirectly to auto-correct meter readings.

There are three distinct approaches that may be taken to model the Coriolis meter within the digital twin: (1) analytical, (2) Timoshenko fluid conveying beam element, or (3) full 3D finite element modeling. Analytical models[21, 22] approximate the Coriolis flow tubes in terms of an equivalent stiffness, damping, and mass. The density and mass flow rate are related to the frequency and phase shift in the meter by analytical equations. These equations involve the use of corrections for the actual geometry of the meter and the weight of the actuator and pickups that are derived from experiments. These models were useful 30 years ago when the cost of computing power was prohibitive, and they do not fully lend themselves to the digital twin paradigm that is based on abundant computing power and good network connectivity.

The Timoshenko beam element approach pioneered by Stack (1993)[23] and later developed by Belhadj et al. (2000)[24], Cheesewright et al. (2003)[25] and Wang et al. (2006)[26] offers the ability to look at the flow tubes in the Coriolis meters in more detail. The effect of the actuator mass, shear deformation of the tubes and calculation of the actual centripetal and Coriolis forces is possible in this approach. Although, the formulation depends on the following assumptions: (a) the tube and the fluid are perfectly coupled, (b) the fluid follows a plugging flow profile, (c) the tubes can be approximated as several straight segments joined together, and (d) space and time variables are separable for the small time step causing the stiffness and damping elements to be time dependent.

The assumption of perfect coupling between the tube and the fluid may underestimate the rotational inertia of the fluid. Therefore, the major effect of the fluid results mostly in a change in the mass per unit length of the beam element. In multiphase flow, it is possible to treat

the fluid as a homogeneous mixture, but errors will be much higher. The assumption of plug flow is valid for single-phase flow, but under multiphase flow, the wavelength of flow pulsation may be shorter, and therefore, it may require even smaller time steps while running the finite element model.

The stiffness, damping, and mass elements in the Timoshenko beam formulation depend on the length of the element used. Curvature in the flow tubes will require a nonuniform mesh. This may require additional computing power to calculate and store a set of stiffness, damping, and mass matrices for every length of the beam element used in the model. Under multiphase flow, the time step for computing the stiffness and damping elements may become unsustainably small — both from computing power and validity perspectives.

The third approach is to use full finite element/volume modeling of the Coriolis meter tubes that couple the fluid elements to the tube's solid elements while solving them individually[27]. This approach is computationally intensive, but can accommodate a wide variety of Coriolis meter designs and flow profiles within them. It has been shown[28] that this approach can be used to examine installation effects through such modeling. It is possible to tie installation effects via 1D pipe flow models before and after the Coriolis meter to fully capture the installation effect while keeping the computational requirement to a minimum.

Digital "Twin" Implementation

Two different implementations of the digital twin Coriolis meter may be envisioned. In the first type of implementation, the raw Coriolis meter measurements are diverted to an edge computer capable of running a simplified Timoshenko beam element model of the meter, Fig. 4. The edge computer can receive additional inputs, from either the Coriolis meter or other sensors such as pressure, temperature, or water cut meters. The edge computer runs the digital twin model constantly and controls the calibration and operation of the Coriolis meter closely while transmitting the corrected mass flow rate and density from the process.

This approach adds to the cost and complexity of an edge computer to each Coriolis meter in the field. The model may not be very powerful and may offer only limited improvements; however, it minimizes the data sent to the cloud and avoids erroneous data from going further. Cleaning data is one of the biggest sources of problems when it comes to data analytics in the oil and gas industry.

In the second embodiment, all the data from the Coriolis meter is sent to the cloud where it is combined with other measurements upstream and downstream of the sensor. A detailed 3D finite element model of the Coriolis meter and its operation may be run on the cloud constantly. Such a "digital twin" of the Coriolis meter may exist within the digital twin of the overall upstream infrastructure and enables the operator to optimize the whole well, field, or reservoir.

To achieve the full benefits of this approach, there is a need for more measurements and more capability within the meter to adapt to changing process conditions. For example, the meter may have to adapt between multiple frequencies of operation[15], based on the feedback from the digital twin. Additional pickups and sensors for monitoring pressure, water cut, tube wall thickness, and corrosion may have to be incorporated into the Coriolis meter itself to give the digital twin the exact usage conditions. The Coriolis meter may also have to be reimagined as a multiphase meter rather than as a single-phase meter adapted to multiphase conditions.

Conclusions

The article outlines the issues with the use of Coriolis meters for multiphase metering. Several approaches to mitigate the errors have been detailed. From the analytical approaches that calculate the error in density and mass flow — due to the presence of gas — to more practical diagnostic algorithms that adapt the drive power, have been described. Subsequently, these approaches may not be able to adapt beyond "entrained gas," which tends to be below 20% of the gas volume fraction within the liquid.

To adapt the Coriolis meter to achieve multiphase metering, a "digital twin" approach has been outlined.

Fig. 4 *Digital Twin on an edge computer.*

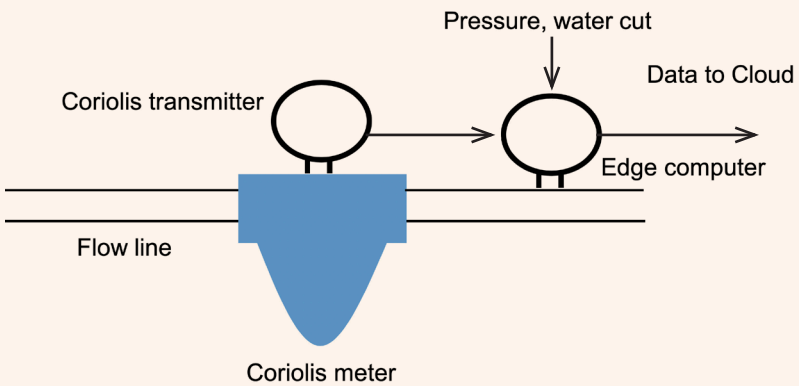

Three approaches to model the Coriolis meter within the digital twin were discussed. Analytical models are already built into existing diagnostic algorithms and have limited potential. Simplified fluid conveying Timoshenko beam elements are useful to look at the meter behavior in more detail, but may still not be capable to fully work under multiphase flow.

A trade-off between computational power and mathematical fidelity may end up satisfying either constraint. A full 3D coupled modeling approach is ideal to achieve a digital twin paradigm, but it is necessary to enable a strong connection between the virtual and real meter. Additional measurements such as pressure, water cut, and tube wall thickness may be necessary, along with considering the installation arrangements upstream and downstream of the meter.

The connection between the real meter and the digital twin must enable a change in the state/operation of both the real and virtual meters. This is needed to allow the two meters to track each other closely and to reap the full benefit of the computational power available today.

Finally, the Coriolis meter design may have to be re-imagined from scratch as a multiphase meter rather than as a single-phase meter adapted for multiphase flow measurement.

Acknowledgments

This article was prepared for presentation at the Offshore Technology Conference, Houston, Texas, May 4-7, 2020.

References

1. Henry, M., Tombs, M., Zamora, M. and Zhou, F.: "Coriolis Mass Flow Metering for Three-Phase Flow: A Case Study," *Flow Measurement and Instrumentation*, Vol. 30, April 2013, pp. 112-122.
2. Basse, N.T.: "A Review of the Theory of Coriolis Flow Meter Measurement Errors due to Entrained Particles," *Flow Measurement and Instrumentation*, Vol. 37, June 2014, pp. 107-118.
3. Henry, M.P., Clarke, D.W., Archer, N., Bowles, J., et al.: "A Self-Validating Digital Coriolis Mass Flow Meter: An Overview," *Control Engineering Practice*, Vol. 8, Issue 5, May 2000, pp. 487-506.
4. Henry, M.P., Duta, M., Tombs, M.S., Yeung, H., et al.: "How a Coriolis Mass Flow Meter can Operate in Two-Phase (Gas/Liquid) Flow," paper presented at the Instrumentation, Systems and Automation Society Show Technical Conference, Houston, Texas, October 5-7, 2004.
5. Hou, Q-L., Xu, K-J., Fang, M., Liu, C., et al.: "Development of Coriolis Mass Flow Meter with Digital Drive and Signal Processing Technology," *ISA Transactions*, Vol. 52, Issue 5, September 2013, pp. 692-700.
6. O'Banion, T.: "Coriolis: The Direct Approach to Mass Flow Measurement," *Chemical Engineering Progress*, Vol. 109, No. 3, 2013, pp. 41-46.
7. Wang, T. and Baker, R.: "Coriolis Flow Meters: A Review of Developments over the Past 20 Years, and an Assessment of the State-of-the-Art and likely Future Directions," *Flow Measurement and Instrumentation*, Vol. 40, December 2014, pp. 99-123.
8. Smith, J.E. and Cage, D.R.: "Parallel Path Coriolis Mass Flow Rate Meter," U.S. Patent No. 4,491,025, 1985.
9. Hemp, J. and Kutin, J.: "Theory of Errors in Coriolis Flow Meter Readings due to Compressibility of the Fluid Being Metered," *Flow Measurement and Instrumentation*, Vol. 17, Issue 6, December 2006, pp. 359-369.
10. Mills, C., Marshall, C., Kay, A. and MacDonald, M.: "Flow Measurement of High Viscosity Fluids," paper presented at the North Sea Flow Measurement Workshop, Tonsberg, Norway, October 2-25, 2013.
11. Tombs, M., Zhou, F. and Henry, M.: "Two-Phase Coriolis Mass Flow Metering with High Viscosity Oil," *Flow Measurement and Instrumentation*, Vol. 59, March 2018, pp. 23-27.
12. Weinstein, J.: "Multiphase Flow in Coriolis Mass Flow Meters — Error Sources and Best Practices," paper presented at the 28th International North Sea Flow Measurement Workshop, October 26-29, 2010.
13. Micro Motion: "Micro Motion Advanced Phase Measurement," Application Manual, MMI-20030076, Rev AC, March 2019, 54 p.
14. Li, M. and Henry, M.: "Complex Signal Processing for Coriolis Mass Flow Metering in Two-Phase Flow," *Flow Measurement and Instrumentation*, Vol. 64, December 2018, pp. 104-115.
15. Endress + Hauser Inc.: "Technical Information Proline Promass Q 300 Coriolis Flow Meter," product information, *www.portal.endress.com*, 88 p.
16. Dasgupta, S. and Kariwala, V.: "ABB's Electromagnetic Flow Meter Digital Twin Drives Performance," *ABB Review*, February 2018, pp. 58-65.
17. Grieves, M. and Vickers, J.: "Digital Twin: Mitigating Unpredictable, Undesirable Emergent Behavior in Complex Systems," in Kahlen, F.J., Flumerfelt, S. and Alves, A. (eds.), *Transdisciplinary Perspectives on Complex Systems*, Springer, 2016, pp. 85-113.
18. Glaessgen, E.H. and Stargel, D.S.: "The Digital Twin Paradigm for Future NASA and U.S. Air Force Vehicles," paper presented at the 53rd Structures, Structural Dynamics and Materials Conference, Honolulu, Hawaii, April 23-26, 2012.
19. Tao, F., Sui, F., Liu, A., Qi, Q., et al.: "Digital Twin-Driven Product Design Framework," *International Journal of Production Research*, Vol. 57, Issue 12, 2019, pp. 3935-3953.
20. Hall, A.R.W. and Reader-Harris, M.J.: "Use of Venturi Meters in Multiphase Flow Measurement," paper presented at the 17th North Sea Flow Measurement Workshop, Gardermoen, Norway, October 25-28, 1999.
21. Sultan, G.: "Theoretical and Experimental Studies of the Coriolis Mass Flow Meter," Ph.D. Thesis, Cranfield University, 1989.
22. Sultan, G. and Hemp, J.: "Modeling of the Coriolis Mass Flow Meter," *Journal of Sound and Vibration*, Vol. 132, Issue 3, August 1989, pp. 473-489.
23. Stack, C.P., Garnett, R.B. and Pawlas, G.E.: "A Finite Element for the Vibration Analysis of a Fluid Conveying Timoshenko Beam," paper presented at the 34th Structures, Structural Dynamics and Materials Conference, La Jolla, California, April 19-22, 1993.
24. Belhadj, A., Cheesewright, R. and Clark, C.: "The Simulation of Coriolis Meter Response to Pulsating Flow Using a General Purpose Finite Element Code," *Journal of Fluids and Structures*, Vol. 14, Issue 5, July 2000, pp. 613-634.

25. Cheesewright, R., Clark, C., Belhadj, A. and Hou, Y.Y.: "The Dynamic Response of Coriolis Mass Flow Meters," *Journal of Fluids and Structures*, Vol. 18, Issue 2, September 2003, pp. 165-178.

26. Wang, S., Clark, C. and Cheesewright, R.: "Virtual Coriolis Flow Meter: A Tool for Simulation and Design," *Proceedings of the Institution of Mechanical Engineers, Part C: Journal of Mechanical Engineering Science*, Vol. 220, Issue 6, 2006, pp. 817-835.

27. Mole, N., Bobovnik, G., Kutin, J., Stok, B., et al.: "An Improved Three-Dimensional Coupled Fluid Structure Model for Coriolis Flow Meters," *Journal of Fluids and Structures*, Vol. 24, Issue 4, May 2008, pp. 559-575.

28. Bobovnik, G., Kutin, J., Mole, N., Stok, B., et al.: "Numerical Analysis of Installation Effects in Coriolis Flow Meters: Single and Twin Tube Configurations," *Flow Measurement and Instrumentation*, Vol. 44, August 2015, pp. 71-78.

About the Authors

Dr. Sakethraman Mahalingam

Ph.D. in Mechanical Engineering, Georgia Institute of Technology

Dr. Sakethraman Mahalingam is a Research Consultant at the Aramco Overseas Company (AOC), Aberdeen, Scotland. Since joining AOC in 2018, his work has been focused on developing new sensors for measuring hydrocarbon flow and composition.

After completing this Ph.D., Sakethraman worked for various divisions of the General Electric Company (GE) and Baker Hughes GE. At GE Global Research, he was instrumental in developing electrical impedance tomography technology for the GE Safire™ multiphase flow meter. At Baker Hughes GE, Sakethraman was involved in the development of subsea sensors and downhole flow and water cut sensors.

He serves as a member of the Committee of Petroleum Measurement at both the American Petroleum Institute (API) and the British Standards Institution (BSI).

Sakethraman is an Associate Editor of the IEEE Transactions on *Components, Packaging and Manufacturing Technology* and the Elsevier *Journal of Measurement.*

He teaches the module on Oil Field Sensors in the M.S. Subsea course at the University of Aberdeen.

Sakethraman has 12 filed patents and over 15 conference and journal articles to his name.

In 2005, he received his Ph.D. degree in Mechanical Engineering from Georgia Institute of Technology, Atlanta, GA.

Dr. Muhammad Arsalan

Ph.D. in Electronics Engineering, Carleton University

Dr. Muhammad Arsalan joined Saudi Aramco in 2013 as a Senior Research Scientist. He is currently leading a team of experts in multiphase metering, sensing, intervention, and robotics focus area within the Production Technology Division of Saudi Aramco's Exploration and Petroleum Engineering Center – Advanced Research Center (EXPEC ARC). Muhammad is also leading the global digital transformation team of EXPEC ARC in advanced sensing domain. His team is working on innovative surface and subsurface production monitoring, control, and optimization technologies.

Muhammad is a seasoned professional with over 20 years of experience in academia and various industries, including biomedical, space, chemicals, and oil and gas. He has over 100 international granted patents and publications related to integrated sensors, systems, and tools.

Muhammad is the recipient of several major national and international awards and distinctions for his entrepreneurial skills and his groundbreaking contributions to the innovation, research and technology development.

Muhammad is the co-founder of two North American technology startups.

In 2004, he was an Invited Researcher and Natural Sciences and Engineering Research Council–Japan Society for the Promotion of Science (NSERC–JSPS) Fellow with the Tokyo Institute of Technology. From 2005 to 2008, Muhammad was an NSERC Alexander Graham Bell Graduate Scholar with the Carleton University.

From 2009 to 2010, he was a National Aeronautics and Space Administration (NASA) postdoctoral Fellow. In 2010, Muhammad joined King Abdullah University of Science and Technology (KAUST) in Thuwal, Saudi Arabia, as an NSERC postdoctoral Research Fellow.

From 2011 to 2016 he was an Adjunct Research Professor with Carleton University, Ottawa, Canada.

Muhammad received his B.Eng. degree from the Institute of Industrial Electronic Engineering, NED University of Engineering and Technology, Karachi, Pakistan in 1999, and his M.S. and Ph.D. degrees, both in Electronic Engineering, from Carleton University, Ottawa, Ontario, Canada, in 2004 and 2009, respectively.